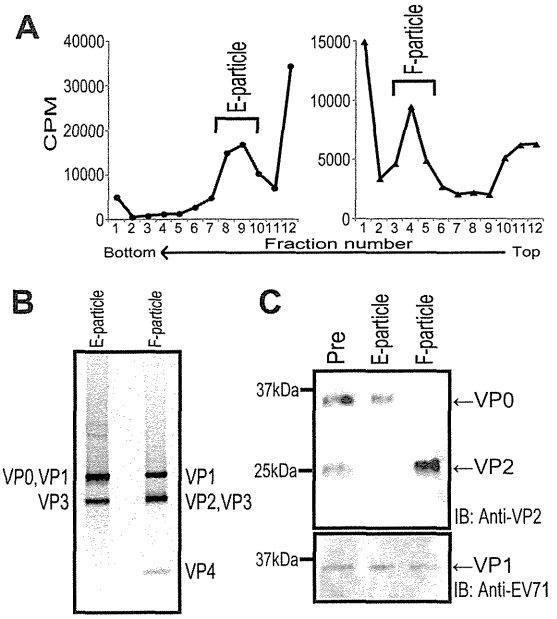

FIG 2 Purification of EV71 F particles. (A) Sucrose density gradient purification of [^{35}S]methionine- and [^{35}S]cysteine-labeled EV71 E particles and F particles. The prepurified E and F particles from the stepwise CsCl gradient centrifugation were layered onto a 15 to 30% sucrose density gradient for ultracentrifugation at 39,000 rpm for 2 h at 4°C. The gradients were fractionated from the top. The E particles (left) and F particles (right) were collected from the indicated fractions. (B) Autoradiography of purified E and F particles. [^{35}S]methionine- and [^{35}S]cysteine-labeled EV71 E particles and F particles (10,000 cpm) were resolved by electrophoresis, and the bands were visualized by autoradiography. (C) Unlabeled E and F particles were resolved by electrophoresis and detected by Western blotting with an anti-VP2 antibody (top) and an anti-EV71 serum that predominantly recognized VP1 (bottom). The positions of the viral proteins are indicated at the sides of the blots. IB, immunoblotting.

Binding of EV71 to SCARB2 and PSGL1. We speculated that the infection efficiency of the cells might be dependent on the amount of virus bound to the cells. We therefore determined the amount of the virus bound to L-SCARB2 cells and L-PSGL1 cells (Fig. 3A). L-Empty cells, L-SCARB2 cells, and L-PSGL1 cells were mixed with 1×10^4, 3×10^4, or 1×10^5 cpm of the ^{35}S-labeled EV71 F particles. After the unbound virions were removed by washing, the cells were lysed with 0.5% SDS and the radioactivity was measured using a liquid scintillation counter. EV71 bound to L-SCARB2 cells and L-PSGL1 cells; however, the amount of EV71 that bound to L-PSGL1 cells was severalfold greater than that bound to L-SCARB2 cells under all tested conditions. These data indicate that more EV71 virion binds to L-PSGL1 cells than to L-SCARB2 cells.

Next, to confirm that EV71 binds to L-PSGL1 cells more efficiently than L-SCARB2 cells, we performed immunofluorescence microscopy to compare the amount of EV71 bound to these cells (Fig. 3B). After the purified EV71 F particles were attached to L-SCARB2 cells or L-PSGL1 cells, the cells were fixed and stained with anti-EV71 serum to detect EV71. Using series of *z*-stack images, we created maximum projections to show three-dimensional information in a plane image. We observed EV71 puncta in L-SCARB2 cells and L-PSGL1 cells, with most of the EV71 being on the surface of the cells. The viral puncta were more intense and more numerous by severalfold in the L-PSGL1 cells than in the

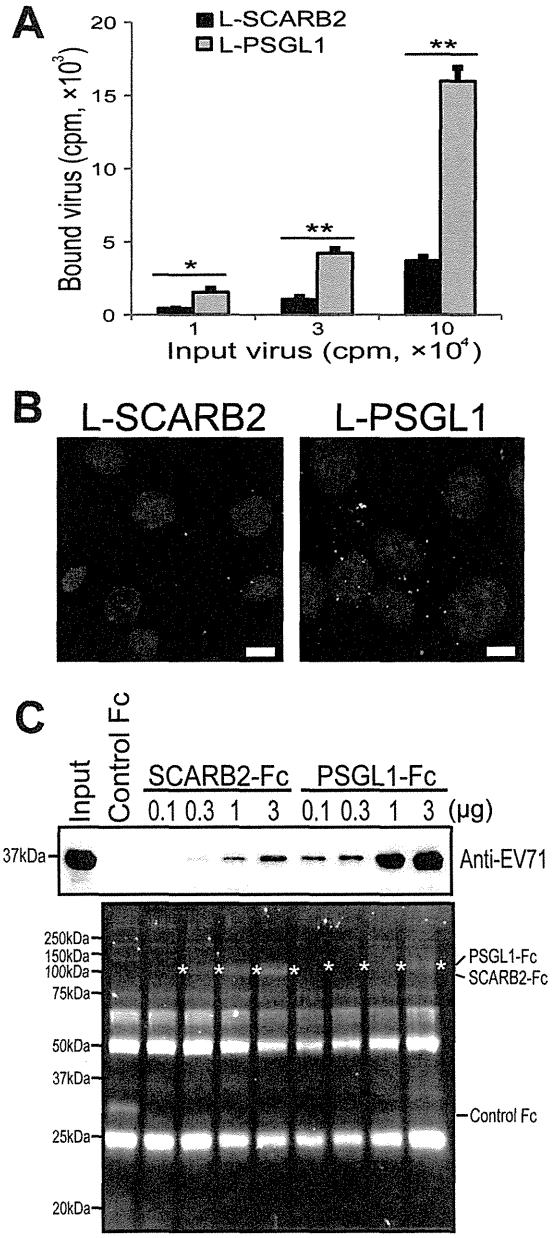

FIG 3 Binding of EV71 to SCARB2 and PSGL1. (A) More EV71 attached to L-PSGL1 cells than to L-SCARB2 cells. L-Empty cells, L-SCARB2 cells, or L-PSGL1 cells were incubated with 1×10^4, 3×10^4, or 1×10^5 cpm of [^{35}S]methionine- and [^{35}S]cysteine-labeled EV71 at 4°C for 2 h. After being washed, the cells were lysed with 0.5% SDS and the amount of bound virion was measured using a liquid scintillation counter. The data are shown as the mean counts with the SDs ($n = 2$). * and **, $P < 0.05$ and $P < 0.01$, respectively, according to Student's *t* test. (B) EV71 attached to L-PSGL1 cells more efficiently than to L-SCARB2 cells, as confirmed by immunofluorescence. EV71 F particles were attached to L-SCARB2 cells or L-PSGL1 cells at 4°C and then at 37°C for 5 min. The cells were washed and fixed before undergoing immunofluorescence microscopy to detect EV71. We analyzed the cells in three-dimensional image stacks by confocal fluorescence microscopy and created a maximum projection. Green indicates EV71, and blue DAPI staining indicates the location of the nuclei. Bars, 10 μm. (C) EV71 bound to SCARB2-Fc and PSGL1-Fc. A total of 10 μg of control Fc and 0.1, 0.3, 1, and 3 μg of SCARB2-Fc and PSGL1-Fc were bound to anti-human Fc-agarose and incubated with EV71. The precipitated proteins were analyzed by Western blotting with the anti-EV71 serum or Oriole gel staining. White asterisks indicate the bands of SCARB2-Fc or PSGL1-Fc.

L-SCARB2 cells. We did not observe any virus dots in the cells without EV71 (data not shown). These results confirm that EV71 F particles bind to L-PSGL1 cells more efficiently than to L-SCARB2 cells.

The results presented above suggested that the amount of PSGL1 expressed on the surface of L-PSGL1 cells is greater than that of SCARB2 expressed on the surface of L-SCARB2 cells and/or the affinity of PSGL1 for EV71 (EV71-PB strain) is greater than that of SCARB2. We then performed a coimmunoprecipitation assay using soluble receptors. EV71 was incubated with various amounts of SCARB2-Fc (extracellular region of SCARB2 fused to the Fc region of human IgG), PSGL1-Fc (extracellular region of PSGL1 fused to the Fc region of human IgG), or control Fc (Fc region of human IgG) bound to anti-Fc agarose beads, and the precipitated proteins were analyzed by Western blotting with an anti-EV71 serum (Fig. 3C, top) and protein staining (Fig. 3C, bottom). The EV71-VP1 band was detected in the 0.3-, 1-, and 3-μg SCARB2-Fc lanes in a concentration-dependent manner and in all of the PSGL1-Fc lanes in a concentration-dependent manner; however, the band was not detected in the control Fc lane or in the 0.1-μg SCARB2-Fc lane. PSGL1-Fc precipitated a larger amount of EV71-VP1 than SCARB2-Fc by severalfold at each concentration of the receptors that we tested. These data suggest that the binding affinity of PSGL1 to EV71 is stronger than that of SCARB2. Taken together, the results indicate that L-PSGL1 cells bind more virus than L-SCARB2 cells due to a higher affinity of PSGL1 for the virus, but the amount of the virus that attached to the cell surface does not solely determine the infection efficiency.

EV71 internalization in L-SCARB2 cells and L-PSGL1 cells. To examine the internalization of purified EV71 virions by L-SCARB2 cells and L-PSGL1 cells, we performed immunofluorescence microscopy (Fig. 4). L-Empty cells, L-SCARB2 cells, or L-PSGL1 cells were incubated with purified EV71 F particles at 4°C, shifted to 37°C, and fixed. The cells were then analyzed by immunofluorescence microscopy to observe EV71 and the early endosome marker EEA1. In the *z*-axis planes where we could observe the internalized virus, we detected EV71 puncta in all L-Empty cells, L-SCARB2 cells, and L-PSGL1 cells at 15 min after the temperature shift to 37°C (Fig. 4A, left). We observed approximately 100 cells for each cell line. There were fewer EV71 signals in the L-Empty cells than in the L-SCARB2 cells and L-PSGL1 cells (average numbers of EV71 puncta in one cell, 0.28, 1.06, and 1.56 for L-Empty cells, L-SCARB2 cells, and L-PSGL1 cells, respectively). The results suggested that the internalization of the virus was enhanced by SCARB2 and PSGL1. In addition, we found that some of the EV71 puncta were colocalized with EEA1 (Fig. 4A, arrowheads), and the number of EV71 puncta that colocalized with EEA1 in L-SCARB2 cells was greater than that in L-PSGL1 cells. For a quantitative comparison of the colocalization of virus puncta with EEA1, we analyzed one *z*-axis midplane per cell, and the numbers of virus puncta colocalized with EEA1 per all virus puncta were as follows: 1 of 33 for L-Empty cells, 8 of 100 for L-SCARB2 cells, and 4 of 89 for L-PSGL1 cells (Fig. 4B). The analysis showed that virus was internalized into the cells and delivered to the early endosome in L-SCARB2 cells, even though a smaller amount of virus attached to L-SCARB2 cells than L-PSGL1 cells.

Conformational alteration of EV71 by SCARB2 under acidic conditions. After the virions are internalized by the cells, the viral genomic RNA must be released from the virion into the cytoplasm

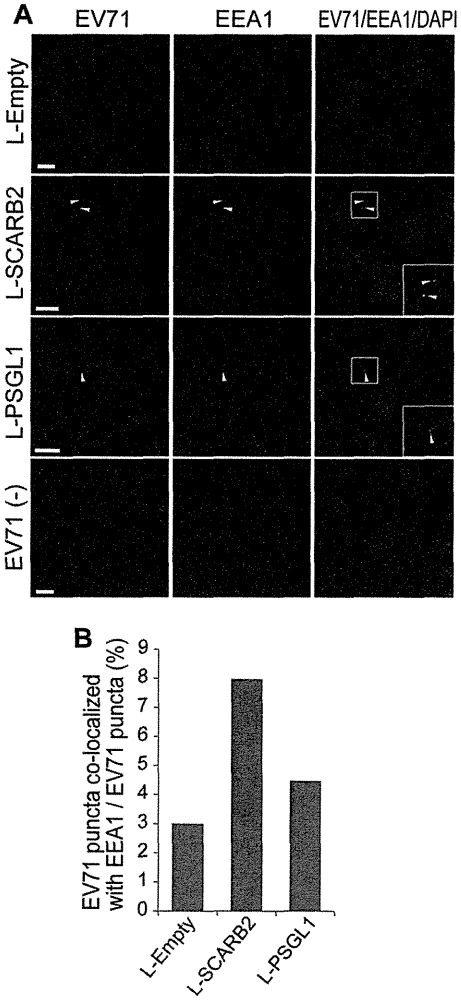

FIG 4 Internalization of EV71 virions into L-SCARB2 cells and L-PSGL1 cells. (A) Immunofluorescence microscopy of EV71 and EEA1 in L-Empty cells, L-SCARB2 cells, and L-PSGL1 cells after incubation with EV71 F particles. The cells were incubated with or without purified F particles at 37°C for 15 min. After the washes, the cells were fixed and stained with or without anti-EV71 and anti-EEA1 antibodies and detected with Alexa Fluor 488- or 568-conjugated secondary antibodies. Green and red indicate EV71 and EEA1, respectively. Blue DAPI staining indicates the location of the nuclei. Arrowheads, colocalization of EV71 with EEA1. (Inset) Enlarged view of the small square. For EV71-negative cells [EV71(−)], we showed L-SCARB2 cells as a representative of L-Empty cells, L-SCARB2 cells, and L-PSGL1 cells because we obtained essentially similar results in all of these cell types. Bars, 10 μm. (B) L-SCARB2 cells internalize EV71 in early endosomes more efficiently than L-Empty cells and L-PSGL1 cells. The ratio of EV71 puncta colocalized with EEA1 compared to EV71 puncta is shown.

to complete the EV71 infection. We expected that SCARB2 could efficiently initiate the uncoating step. To analyze the conformational alteration of EV71 as a mimic of the uncoating step by sucrose density gradient ultracentrifugation, we prepared EV71 empty capsids by heating the purified F particles; these served as a reference (Fig. 5A). As another control, we also prepared PV A particles and empty capsids by incubating native PV virions with PVR (Fig. 5B). According to the sucrose density gradient ultracentrifugation, the EV71 and PV native virions sedimented at fractions 6 to 8 (native virion), the heat-treated EV71 sedimented at fractions 14 and 15 (empty capsid), and PV, which was treated

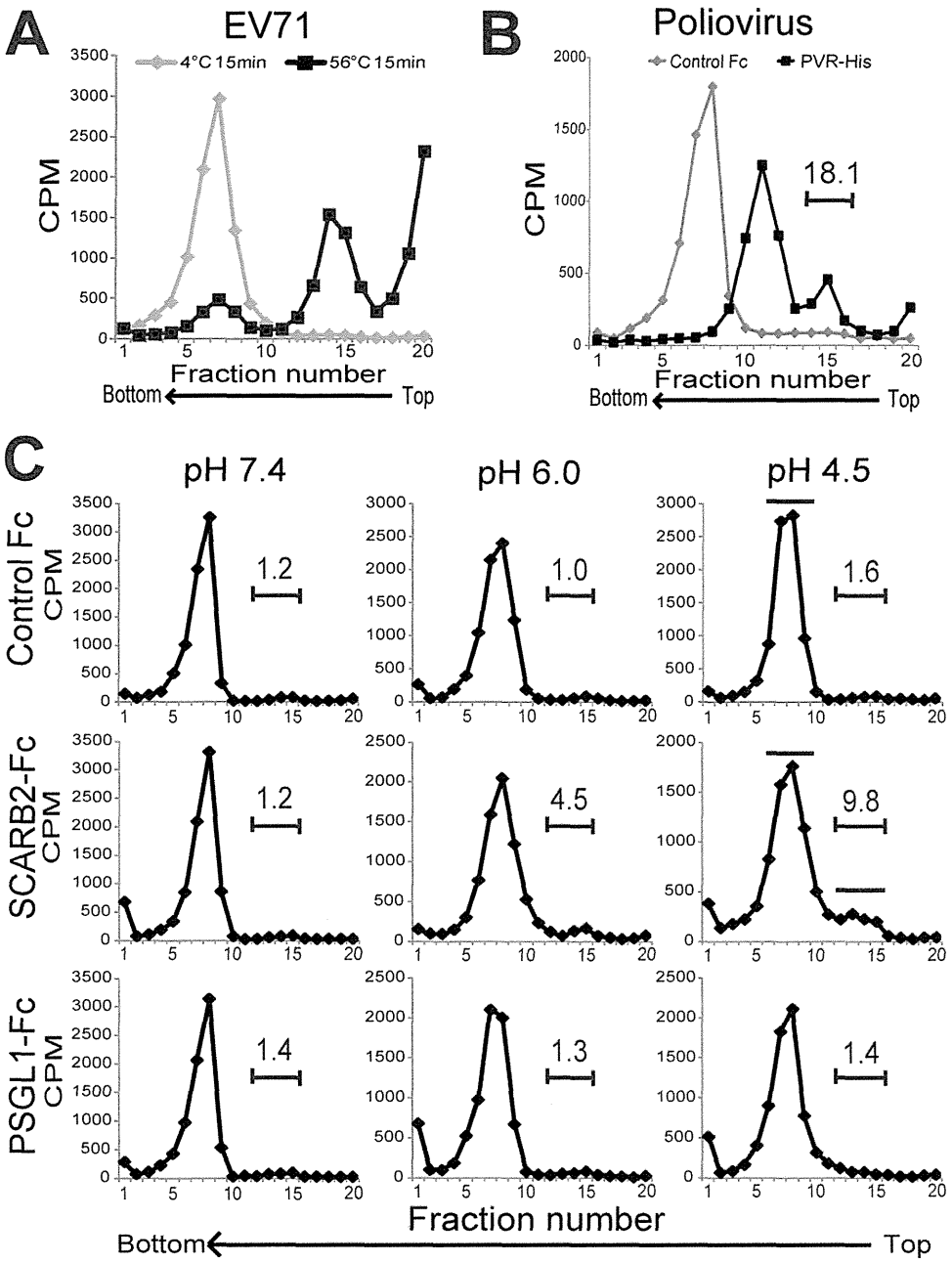

FIG 5 Conformational alteration of EV71 by SCARB2 under an acidic pH. (A) Characterization of EV71 F particles and heat-induced empty capsids by ultracentrifugation. Approximately 10,000 cpm of purified F particles was incubated for 15 min at 4°C or 56°C. The samples were centrifuged in 15 to 30% sucrose gradients, and the radioactivity of each fraction (0.6 ml) was measured by liquid scintillation counting. (B) Native virion, A particle, and empty capsid of PV. Approximately 10,000 cpm of the PV native virion was treated with 1 μg of PVR-His and control Fc for 1 h at 4°C and subsequently incubated for 1 h at 37°C. The samples were analyzed using 15 to 30% sucrose gradients. The number above the bracketed line indicates the proportion of fractions 14 to 16. (C) Conformational alteration of EV71 F particles via incubation with SCARB2-Fc at various pH levels. Approximately 10,000 cpm of purified F particles was treated with 1 μg of control Fc, 1 μg of SCARB2-Fc, or 1 μg of PSGL1-Fc for 60 min at 4°C and then incubated for 60 min at 37°C at a pH of 7.4, 6.0, or 4.5. The samples were analyzed using 15 to 30% sucrose gradients. The numbers above the bracketed lines indicate the proportions of fractions 12 to 15. The fractions indicated by solid bars were collected and used for analysis of VP4 and viral RNA in Fig. 6.

with PVR, sedimented at fractions 10 to 12 (A particle) and fractions 14 to 16 (empty capsid, approximately 18.1% of total counts). These results indicate that the empty capsids of EV71 appeared as a peak in fractions 14 and 15 and that the A particles appeared as a peak in fractions 10 to 12.

To analyze the conformational alteration of EV71, EV71 was incubated with 1 μg of control Fc, SCARB2-Fc, or PSGL1-Fc at 37°C at pH 7.4, 6.0, or 4.5 and subjected to sucrose density gradient ultracentrifugation (Fig. 5C). The peak of the native virion (fractions 6 to 10) did not shift when the F particles were incubated with control Fc or PSGL1-Fc at any pH, whereas a portion of the ^{35}S-labeled virions (approximately 4.5% and 9.8% of total

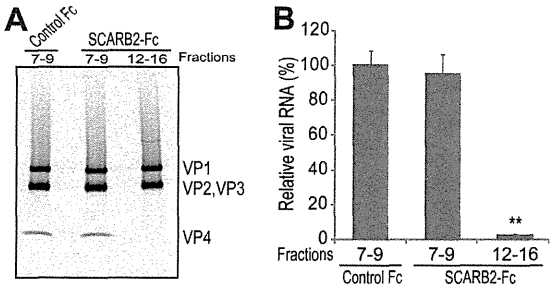

FIG 6 Release of VP4 and viral RNA. (A) Release of VP4 by treatment with SCARB2-Fc. Approximately 10,000 cpm of virus particles from fractions 7 to 9 and 12 to 15 of SCARB2-Fc-treated EV71 and from fractions 7 to 9 of control Fc-treated EV71 were collected and analyzed by SDS-PAGE and subsequent autoradiography. (B) Contents of viral RNA. The viral RNA was extracted from approximately 500 cpm of each sample. The viral RNA was quantified by quantitative RT-PCR ($n = 3$). The data are shown as the relative proportions of viral RNA with the SDs ($n = 3$). The contents of the viral RNA in fractions 7 to 9 of control Fc were set to 100%. **, $P < 0.01$ by Student's t test.

counts at pH 6.0 and pH 4.5, respectively) formed a shoulder peak at fractions 12 to 15 when incubated with SCARB2-Fc at an acidic pH but not under neutral conditions at pH 7.4. These data indicate that the conformational alteration of EV71 is triggered by incubation with SCARB2 under acidic conditions.

Release of VP4 and viral genomic RNA from native virions. Because a portion of the EV71 virions shifted to the fractions that sedimented at a lower rate after incubation with SCARB2 under acidic conditions, we determined whether the viral particles in fractions 12 to 15 contained VP4 and/or viral genomic RNA. For this purpose, we collected fractions 7 to 9 of the control Fc-treated EV71 and fractions 7 to 9 and 12 to 15 of SCARB2-Fc-treated EV71 (the collected fractions are indicated by solid bars in Fig. 5C). To analyze VP4, approximately 10,000 cpm of each sample was separated by SDS-PAGE and imaged with a phosphorimaging plate (Fig. 6A). VP4 together with VP1, VP2, and VP3 was clearly detected in each lane of fractions 7 to 9 of the control Fc- or SCARB2-Fc-treated EV71. VP4 was not detected in fractions 12 to 15 of SCARB2-Fc-treated EV71, whereas VP1, VP2, and VP3 were detected at levels that were similar to those in the other lanes. For the viral genomic RNA analysis, viral genomic RNA was extracted from approximately 500 cpm of each sample and quantified using real-time RT-PCR (Fig. 6B). The levels of viral genomic RNA in fractions 7 to 9 of SCARB2-Fc-treated EV71 were comparable to the levels in fractions 7 to 9 of the control Fc-treated EV71. The amount of viral genomic RNA in fractions 12 to 15 of the SCARB2-Fc-treated EV71 was significantly reduced compared with that in fractions 7 to 9 of the control Fc-treated EV71 ($P = 0.00190$). Taken together, these data demonstrate that the particles in fractions 12 to 15 of the SCARB2-Fc-treated EV71 are empty capsids.

Time course and pH dependency of the conformational alteration of EV71 by SCARB2. We evaluated the dependency of the conformational alteration on the incubation time and pH. First, to evaluate the time course of the conformational alteration, the native virions that bound to SCARB2-Fc were incubated at 37°C for 0, 0.5, 1, 2, or 3 h at pH 4.5 and analyzed by use of a sucrose density gradient (Fig. 7A). The empty capsid in fractions 11 to 15 was observed after incubation for 0.5 h. The proportion of these fractions increased from 0.7% (0 h) to 13.3% (0.5 h), 18.6% (1 h), 19.5% (2 h), and 21.1% (3 h) in a time-dependent manner. The proportion of virus that sedimented with fractions 11 to 15 after incubation of native virions with control Fc at 37°C for 3 h at pH 4.5 was 1.7%. These data indicate that the conformational change of EV71 is induced in a time-dependent manner. However, not all of the virions were converted into empty capsids after the longer incubation periods.

Second, to evaluate the pH dependency of the conformational alteration, we incubated the native virions that bound to SCARB2-Fc at 37°C for 1 h at pH 7.4, 6.5, 6.0, 5.5, 5.0, or 4.5 and subjected them to sucrose density gradient ultracentrifugation (Fig. 7B). The conformational alteration from the native virion to the empty capsid was induced in a pH-dependent manner; empty capsid formation was rarely observed at pH 7.4 and 6.5 (approximately 1.2% and 2.6%, respectively), whereas a conformational alteration was observed at pH 6.0, 5.5, 5.0, and 4.5 (approximately 5.0, 6.1, 6.5, and 8.1%, respectively). Consistent with these data, we confirmed that infection of RD cells by EV71 was inhibited by pretreatment with NH_4Cl, an endosome acidification inhibitor, as previously reported (24–26). Infection of L-PSGL1 cells with EV71 was also inhibited by the same treatment, but infection with PV was not affected (data not shown). Thus, these data suggest that the conformational alteration, an essential step in EV71 entry, requires an acidic pH below 6.0.

Because we used EV71 strain SK-EV006 (genogroup B), which binds to both SCARB2 and PSGL1, for the conformation alteration assays, we performed a conformation alteration assay with EV71 strain BrCr (genogroup A), which binds only to SCARB2, and strain 1095 (genogroup C), which binds to SCARB2 and PSGL1 (data not shown) (18). The purified BrCr and 1095 F particles were incubated with 1 μg of control Fc, SCARB2-Fc, or PSGL1-Fc at 37°C at pH 4.5 and subjected to a sucrose density gradient (Fig. 7C). In both cases, the major peak (fractions 5 to 8) of the native virion did not shift when the native virions were incubated with control Fc or PSGL1-Fc, whereas a portion of the native virions shifted to fractions 10 to 15 and formed a shoulder peak when incubated with SCARB2-Fc. Because the conformational alteration of three strains from genogroups A, B, and C was confirmed, we suggest that the conformational alteration of EV71 is generally mediated by SCARB2 in an acidic pH.

Uncoating of EV71 in L-SCARB2 cells. To confirm that the same conformational alteration of EV71 occurs *in vivo*, we performed conformational alteration assays with virus associated with L-SCARB2 cells or L-PSGL1 cells (Fig. 8). The ^{35}S-labeled EV71 attached to L-SCARB2 cells or L-PSGL1 cells was incubated for 0.5, 1, or 2 h at 37°C, and the conformational state of the EV71 virions was analyzed by sucrose density gradient ultracentrifugation (Fig. 8). Empty capsids formed a peak at fractions 13 to 15 when native virions were incubated with L-SCARB2 cells, and the proportion in the empty capsid fraction was increased from 5.7% (0.5 h) to 8.1% (1 h) and 17.6% (2 h) in a time-dependent manner. The distinct shift of the native virion peak (fractions 4 to 10) was not observed when the EV71 native virions were incubated with L-PSGL1 cells at any of the time points tested. These data indicate that the uncoating of EV71 occurs in L-SCARB2 cells.

DISCUSSION

For the establishment of enterovirus infection, the virus must bind to the surface of target cells, enter into the cells (this step may not be necessary in some picornaviruses), and release viral genomic

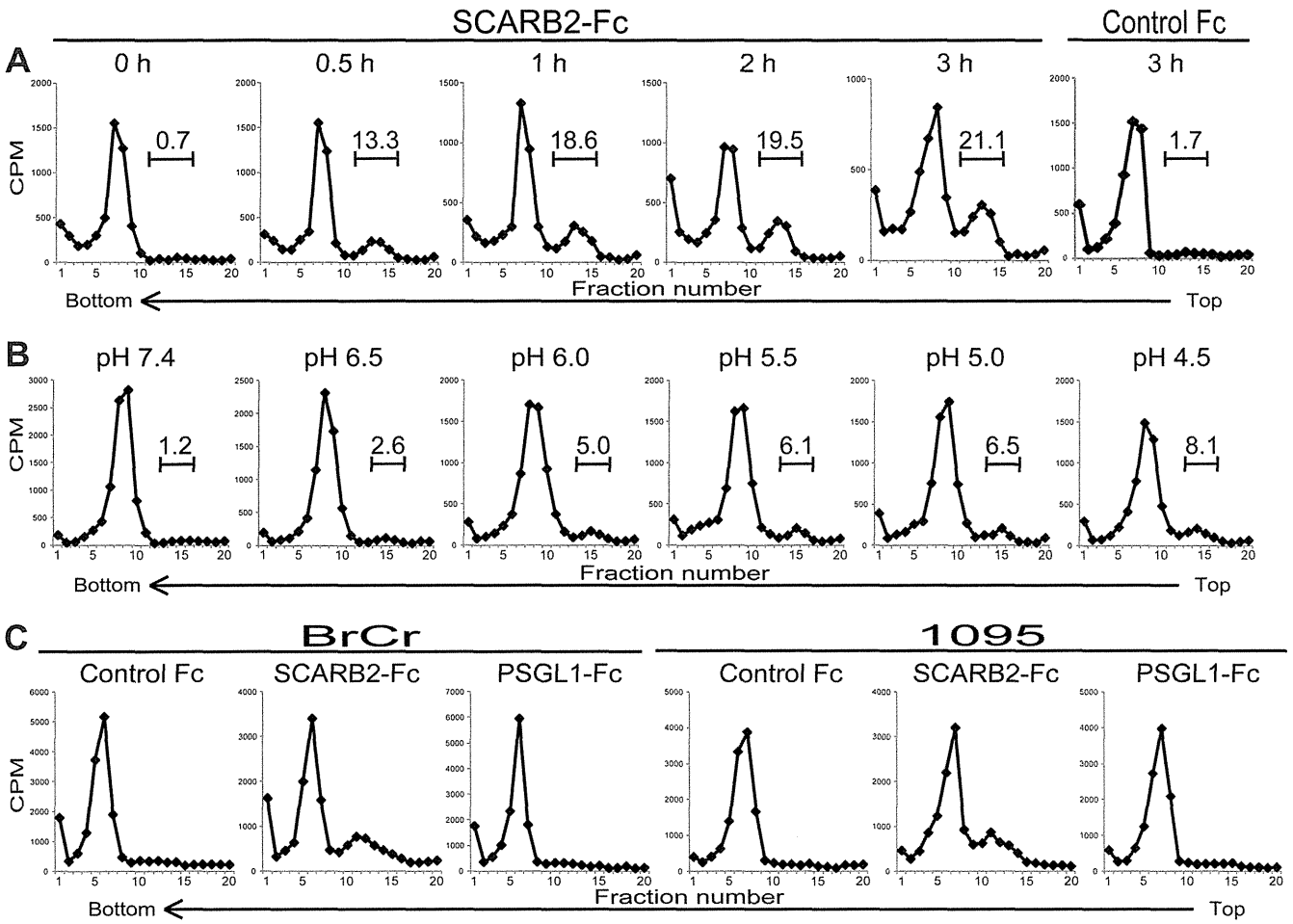

FIG 7 Effect of incubation time, pH, and EV71 strains on the conformational alteration of EV71 in the presence of SCARB2. (A) Incubation time-dependent conformational alteration of EV71. EV71 was treated with 1 μg of SCARB2-Fc for 0, 0.5, 1, 2, and 3 h or 1 μg of control-Fc for 3 h at pH 4.5 at 37°C and analyzed by sucrose gradient centrifugation. The numbers above the bracketed lines indicate the proportions of fractions 11 to 15. (B) pH-dependent conformational alteration of EV71. [^{35}S]methionine- and [^{35}S]cysteine-labeled EV71 F particles were incubated with 1 μg of SCARB2-Fc at pH 7.4, 6.5, 6.0, 5.5, 5.0, and 4.5 at 37°C, and the conformational alterations were analyzed at 1 h by sucrose density gradient centrifugation. The numbers above the bracketed lines indicate the proportions of fractions 13 to 16. (C) Conformational alteration of other strains of EV71 by SCARB2. [^{35}S]methionine- and [^{35}S]-cysteine-labeled EV71 strains BrCr (genogroup A) and 1095 (genogroup C) were incubated with 1 μg of control Fc, 1 μg of SCARB2-Fc, and 1 μg of PSGL1-Fc at pH 4.5 at 37°C for 1 h, and the conformational alterations were analyzed by sucrose density gradient centrifugation.

RNA into the cytoplasm. The viral receptor promotes infection by playing multiple roles, including viral attachment, internalization, and uncoating. It has been independently reported that the receptors SCARB2 and PSGL1 bind to the EV71 virion and mediate EV71 infection (17, 18, 22–24, 26, 31, 63). We have demonstrated that SCARB2 supports EV71 infection in nonsusceptible cells more efficiently than PSGL1, despite the reduced binding ability of SCARB2 to the EV71 virion compared to that of PSGL1.

We first compared the virus-binding capacities of SCARB2 and PSGL1. Unexpectedly, L-PSGL1 cells could bind to more viruses than L-SCARB2 cells (Fig. 3A and B), and soluble PSGL1 could bind to more viruses than SCARB2 (Fig. 3C). The capacity of SCARB2 binding to EV71 was lower than that of PSGL1. Regions on the EV71 virion that are important for the interaction with SCARB2 and PSGL1 have been identified. The glutamine residue at position 172 in the EF loop region of VP1, which lines the wall of the canyon on the viral surface, was important for binding to SCARB2, suggesting that SCARB2 binds inside the canyon (24). Recently, structural data were collected and revealed that the canyon of EV71 is shallower than that of other enteroviruses (3, 4). It is well-known that uncoating receptors, such as PVR, CAR, and ICAM-1, have immunoglobulin-like domains and bind to the viral canyon (33). However, SCARB2 does not have immunoglobulin-like domains. We have previously demonstrated that amino acids 142 to 204 of SCARB2 are important for the interaction with EV71 (23). Thus, this region of SCARB2 may fit the shallow canyon. Regarding PSGL1, VP2 residue 149 participates in forming the puff that serves as the southern rim of the canyon (4) and is important for PSGL1-EV71 binding (18, 63). These findings suggest that SCARB2 and PSGL1 bind at different sites on the virion and that the affinity of the SCARB2-EV71 interaction is different from that of the PSGL1-EV71 interaction.

The discrepancy between the infection efficiency and binding suggests that SCARB2 plays additional essential roles in the internalization and/or induction of viral uncoating, the step after viral attachment. We first examined whether EV71 was internalized via

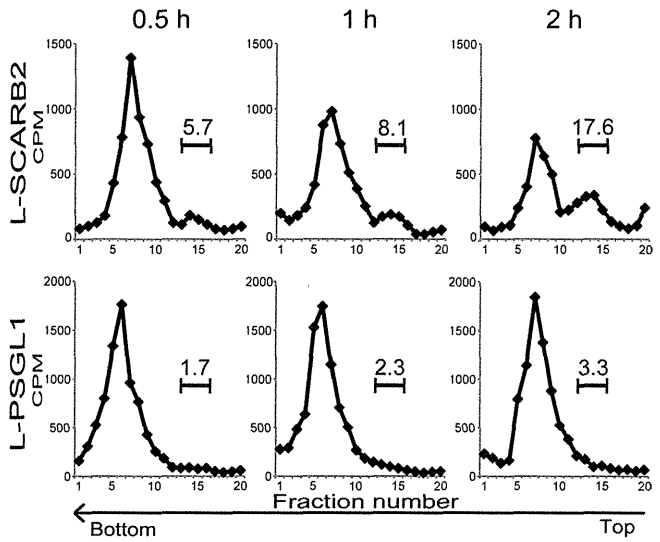

FIG 8 Conformational alteration of EV71 in L-SCARB2 cells. Purified EV71 F particles bound to L-SCARB2 cells and L-PSGL1 cells were incubated for 0.5, 1, or 2 h at 37°C. The cells were lysed with 1% Triton X-100, and these lysates were analyzed using 15 to 30% sucrose gradients. The numbers above the bracketed lines indicate the proportions of fractions 13 to 15.

a SCARB2- or PSGL1-dependent pathway (Fig. 4). We observed internalized viruses in both L-SCARB2 cells and L-PSGL1 cells. In some instances, the EV71 puncta colocalized with the endosome marker. The amount of virus associated with endosomes in L-SCARB2 cells is greater than that in L-PSGL1 cells. SCARB2 is normally present in lysosomes and shuttles via vesicular transport to the plasma membrane through endosomes (19). It is likely that SCARB2 captures EV71 when SCARB2 is present at the plasma membrane. SCARB2 on the cell surface is transported to lysosomes by clathrin-mediated endocytosis (19). EV71 infects RD cells via the SCARB2-dependent pathway (22, 26). EV71 infection of RD cells was inhibited by knocking down the expression of the clathrin heavy peptide (CLTC) by treatment with chlorpromazine, an inhibitor of clathrin-mediated endocytosis, and by the expression of a dominant-negative mutant, EPS15 (25). The inhibition of EV71 infection by a depletion of clathrin-mediated endocytosis was similarly observed in mouse 3T3 cells that expressed human SCARB2 (26). These reports, together with our data, suggest that SCARB2 plays a role in internalizing the viral particles and delivering them to the endosome using the physiological pathway of SCARB2. Our data showed that at least a portion of the viruses that were internalized via the SCARB2 pathway was delivered to the endosome, where the viruses were exposed to an acidic pH. It is therefore likely that the EV71 puncta that colocalized with the endosomal marker represent the viruses that are involved in a productive stage of infection. However, the precise mechanisms of EV71 entry via SCARB2 should be studied more in detail.

Next, we performed a conformational alteration assay with ^{35}S-labeled EV71 to determine whether SCARB2 or PSGL1 induces the uncoating process (Fig. 5). A particles and empty capsids are considered to be important intermediates and end products, respectively, during the uncoating process. Therefore, detecting these particles is important in order to confirm the role of these two receptors in the uncoating process. The empty capsids were generated by incubating the native virions with SCARB2 but not with PSGL1 both *in vitro* and *in vivo*. Recently, the crystal structure of the EV71 E particle was reported with high resolution (3, 4). The E particle of EV71 has properties similar to those of the PV and HRV empty capsids, as determined by cryo-electron microscopy and X-ray diffraction (64, 65). Therefore, it is possible that the empty capsid of EV71 also has exits for viral genomic RNA near the 2-fold axis. We demonstrated that the conformation of the EV71 virion was altered by incubation with soluble SCARB2 under acidic conditions (Fig. 5C). Consistent with these results, previous studies have found that EV71 entry via the SCARB2-dependent pathway was inhibited by endosome acidification inhibitors (24–26). Soluble PSGL1 did not induce a conformational change under any tested physiological pH. Taken together, these data demonstrate that SCARB2 functions as an uncoating receptor during EV71 entry, and this property is a major reason that L-SCARB2 cells support an efficient EV71 infection compared with the efficiency of infection for L-PSGL1 cells. Because SCARB2 shuttles between lysosomes and the plasma membrane (19), the EV71-SCARB2 complex that is formed at the plasma membrane may enter the endosomal compartment, in which the complex is then exposed to an acidic pH. A viral conformation alteration occurred when the pH was less than 6.0 in the cell-free system (Fig. 7B), suggesting that the uncoating events begin in the early endosomes.

To date, several patterns of uncoating processes have been reported for picornaviruses. One pattern is the conformational alteration of PV, CVB, and the major-group HRVs, which is facilitated by PVR, CAR, and ICAM-1, respectively (Fig. 9A) (34, 46, 48). The native virions of PV, CVB and the major-group HRVs treated with respective receptors become A particles after releasing VP4 at neutral pH. The A particle becomes an empty capsid after releasing viral RNA. In the case of HRV14 and HRV16, the alteration is dependent on ICAM-1 and low pH (53). Another pattern is the conformational alteration of the minor-group HRVs, which is dependent on an acidic pH (Fig. 9B) (34, 50). VP4 and viral RNA are sequentially released from the native virion under an acidic environment because both A particles and empty capsids were detected. In addition, the other pattern of conformational alteration in aphthovirus also depends on an acidic pH (Fig. 9B) (34, 51). Under acidic conditions, the native virion dissociates into an empty capsid and then into pentameric subunits for viral RNA release. In this study, we revealed that the conformational alteration of EV71 is different from these patterns and requires both SCARB2 and an acidic pH (Fig. 9C). Additionally, we observed the formation of empty capsids but not A particles (Fig. 5 and 6). Therefore, either the native EV71 virion is converted directly into an empty capsid or the A particles were not detected because they have a short half-life. Chen et al. performed a conformational alteration assay by monitoring the shift of the viral RNA peak using purified EV71 and soluble receptors (24). In contrast to our findings, they observed the formation of an RNA peak that sedimented at a lower rate than the native virion (24). Chen et al. claimed that the shifted viral RNA peak was representative of A particles; however, they did not demonstrate whether VP4 existed in putative A-particle fractions or whether empty capsids were formed (24). In either case, the mode of EV71 conformational alteration is a novel pattern among picornaviruses because both SCARB2 and an acidic pH are essential for conformational alteration.

We have demonstrated that PSGL1 binds to a large amount of

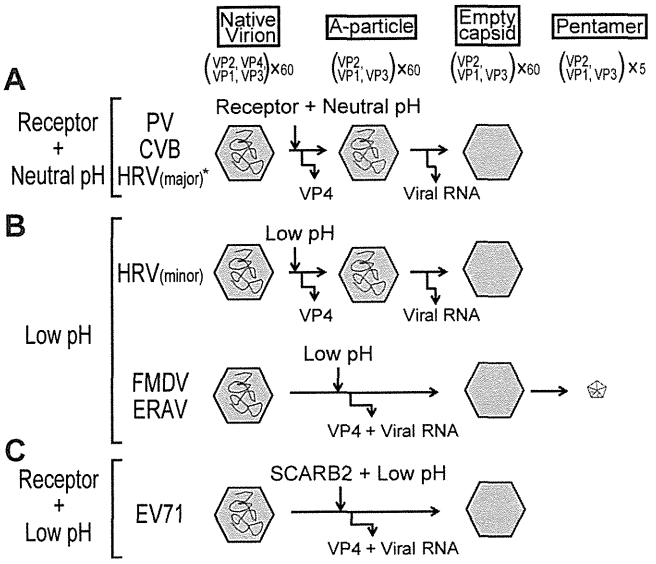

FIG 9 Schematic diagrams of the conformational alterations of picornaviruses. (A) Receptor-dependent conformational alteration at a neutral pH pattern. The conformational alteration of PV, CVB, and the major-group HRVs is triggered by their respective receptors at a neutral pH. The native virion becomes an A particle when VP4 is released from the native virion. The A particle becomes an empty capsid when the viral RNA is released from the A particle. *, HRV14 and HRV16 require both receptor and low pH. (B) Low-pH-dependent conformational alteration pattern. The conformational alteration is triggered by an acidic environment. VP4 and the viral RNA of the minor-group HRVs are released sequentially in a pattern similar to that in panel A. The conformational alteration of FMDV and ERAV is also triggered by an acidic pH. The native virion releases both VP4 and viral RNA and changes into empty capsid and then into pentamers. In the case of FMDV uncoating, the existence of an empty capsid has not been proven. (C) Receptor-dependent conformational alteration at a low pH pattern. The conformational alteration of EV71 is triggered by the receptor SCARB2 under an acidic pH. VP4 and viral RNA are released from the native virion, and the native virion directly becomes an empty capsid.

EV71 (a PB strain) but does not induce conformational alterations. This situation is similar to the DAF in CVB receptors. DAF binds to several strains of CVB and does not induce conformational alterations (33). Because DAF functions only as a binding factor, an additional molecule, CAR, is needed to establish an efficient infection through the DAF-dependent pathway. However, in polarized epithelial cells, CAR is exclusively located in the tight junctions and is not directly accessible. Thus, DAF-mediated signals permit the virus to move across the apical cell surface to the tight junction, where they can interact with CAR (47). The virus captured by PSGL1 may be similarly uncoated by SCARB2 in human cells that expressed both receptors or by unknown molecules if SCARB2 is absent.

The data suggest that SCARB2 is an authentic receptor for EV71. Only EV71 PB strains have adapted to use PSGL1 as a receptor. The evolutionary significance of using PSGL1 as a receptor is not presently clear. PSGL1 might contribute by broadening the target cells *in vivo*. It may also act as more than an attachment site on the cell surface. The infection of lymphocytes may trigger the induction of proinflammatory cytokines and participate in pathogenesis because individuals with severe EV71-associated encephalitis and neurogenic pulmonary edema have exhibited high levels of proinflammatory cytokines (66, 67). Further analyses are needed to evaluate the role of PSGL1 as a receptor for EV71.

In summary, we compared SCARB2 and PSGL1 as EV71 receptors. These two receptors demonstrated different abilities in viral attachment, internalization, and uncoating. SCARB2 plays all three roles, whereas PSGL1 does not have the ability to initiate EV71 uncoating. Therefore, PSGL1 alone is not sufficient to enhance EV71 infection in mice (32). Our preliminary results suggest that the transgenic expression of SCARB2 is sufficient to cause neurological diseases in mice. The mouse model that expresses human SCARB2 will greatly contribute to the understanding of EV71 neuropathogenicity *in vivo* and the development of a vaccine and/or antiviral drugs.

ACKNOWLEDGMENTS

We thank H. Shimizu (NIDD of Japan) for helpful discussions.

This work was supported in part by a Grant-in-Aid for Scientific Research (B) (23390116) and a Grant-in-Aid for Scientific Research (C) (23590557) from the Japan Society for the Promotion of Science and in part by a Grant-in-Aid for Research on Emerging and Re-Emerging Infectious Diseases from the Ministry of Health, Labor and Welfare, Japan.

REFERENCES

1. **Racaniello V.** 2007. Picornaviridae: the viruses and their replication, p 795–838. *In* Knipe DM, Howley PM, Griffin DE, Lamb RA, Martin MA, Roizman B, Straus SE (ed), Fields virology, 5th ed. Lippincott Williams & Wilkins, Philadelphia, PA.
2. **Rossmann MG, Johnson JE.** 1989. Icosahedral RNA virus structure. Annu. Rev. Biochem. **58**:533–573.
3. **Wang X, Peng W, Ren J, Hu Z, Xu J, Lou Z, Li X, Yin W, Shen X, Porta C, Walter TS, Evans G, Axford D, Owen R, Rowlands DJ, Wang J, Stuart DI, Fry EE, Rao Z.** 2012. A sensor-adaptor mechanism for enterovirus uncoating from structures of EV71. Nat. Struct. Mol. Biol. **19**:424–429.
4. **Plevka P, Perera R, Cardosa J, Kuhn RJ, Rossmann MG.** 2012. Crystal structure of human enterovirus 71. Science **336**:1274.
5. **Rossmann MG, He Y, Kuhn RJ.** 2002. Picornavirus-receptor interactions. Trends Microbiol. **10**:324–331.
6. **Schmidt NJ, Lennette EH, Ho HH.** 1974. An apparently new enterovirus isolated from patients with disease of the central nervous system. J. Infect. Dis. **129**:304–309.
7. **Blomberg J, Lycke E, Ahlfors K, Johnsson T, Wolontis S, von Zeipel G.** 1974. New enterovirus type associated with epidemic of aseptic meningitis and-or hand, foot, and mouth disease. Lancet **ii**:112.
8. **Hagiwara A, Tagaya I, Yoneyama T.** 1978. Epidemic of hand, foot and mouth disease associated with enterovirus 71 infection. Intervirology **9**:60–63.
9. **McMinn PC.** 2002. An overview of the evolution of enterovirus 71 and its clinical and public health significance. FEMS Microbiol. Rev. **26**:91–107.
10. **Fujimoto T, Chikahira M, Yoshida S, Ebira H, Hasegawa A, Totsuka A, Nishio O.** 2002. Outbreak of central nervous system disease associated with hand, foot, and mouth disease in Japan during the summer of 2000: detection and molecular epidemiology of enterovirus 71. Microbiol. Immunol. **46**:621–627.
11. **Chan LG, Parashar UD, Lye MS, Ong FG, Zaki SR, Alexander JP, Ho KK, Han LL, Pallansch MA, Suleiman AB, Jegathesan M, Anderson LJ.** 2000. Deaths of children during an outbreak of hand, foot, and mouth disease in Sarawak, Malaysia: clinical and pathological characteristics of the disease. For the Outbreak Study Group. Clin. Infect. Dis. **31**:678–683.
12. **Ho M, Chen ER, Hsu KH, Twu SJ, Chen KT, Tsai SF, Wang JR, Shih SR.** 1999. An epidemic of enterovirus 71 infection in Taiwan. Taiwan Enterovirus Epidemic Working Group. N. Engl. J. Med. **341**:929–935.
13. **Ahmad K.** 2000. Hand, foot, and mouth disease outbreak reported in Singapore. Lancet **356**:1338.
14. **Qiu J.** 2008. Enterovirus 71 infection: a new threat to global public health? Lancet Neurol. **7**:868–869.
15. **Yan JJ, Wang JR, Liu CC, Yang HB, Su IJ.** 2000. An outbreak of enterovirus 71 infection in Taiwan 1998: a comprehensive pathological, virological, and molecular study on a case of fulminant encephalitis. J. Clin. Virol. **17**:13–22.
16. **Yang F, Ren L, Xiong Z, Li J, Xiao Y, Zhao R, He Y, Bu G, Zhou S,**

Wang J, Qi J. 2009. Enterovirus 71 outbreak in the People's Republic of China in 2008. J. Clin. Microbiol. 47:2351–2352.
17. Yamayoshi S, Yamashita Y, Li J, Hanagata N, Minowa T, Takemura T, Koike S. 2009. Scavenger receptor B2 is a cellular receptor for enterovirus 71. Nat. Med. 15:798–801.
18. Nishimura Y, Shimojima M, Tano Y, Miyamura T, Wakita T, Shimizu H. 2009. Human P-selectin glycoprotein ligand-1 is a functional receptor for enterovirus 71. Nat. Med. 15:794–797.
19. Eskelinen EL, Tanaka Y, Saftig P. 2003. At the acidic edge: emerging functions for lysosomal membrane proteins. Trends Cell Biol. 13:137–145.
20. Reczek D, Schwake M, Schroder J, Hughes H, Blanz J, Jin X, Brondyk W, Van Patten S, Edmunds T, Saftig P. 2007. LIMP-2 is a receptor for lysosomal mannose-6-phosphate-independent targeting of beta-glucocerebrosidase. Cell 131:770–783.
21. Blanz J, Groth J, Zachos C, Wehling C, Saftig P, Schwake M. 2010. Disease-causing mutations within the lysosomal integral membrane protein type 2 (LIMP-2) reveal the nature of binding to its ligand beta-glucocerebrosidase. Hum. Mol. Genet. 19:563–572.
22. Yamayoshi S, Iizuka S, Yamashita T, Minagawa H, Mizuta K, Okamoto M, Nishimura H, Sanjoh K, Katsushima N, Itagaki T, Nagai Y, Fujii K, Koike S. 2012. Human SCARB2-dependent infection by coxsackievirus A7, A14, and A16 and enterovirus 71. J. Virol. 86:5686–5696.
23. Yamayoshi S, Koike S. 2011. Identification of a human SCARB2 region that is important for enterovirus 71 binding and infection. J. Virol. 85: 4937–4946.
24. Chen P, Song Z, Qi Y, Feng X, Xu N, Sun Y, Wu X, Yao X, Mao Q, Li X, Dong W, Wan X, Huang N, Shen X, Liang Z, Li W. 2012. Molecular determinants of enterovirus 71 viral entry: cleft around GLN-172 on VP1 protein interacts with variable region on scavenge receptor B 2. J. Biol. Chem. 287:6406–6420.
25. Hussain KM, Leong KL, Ng MM, Chu JJ. 2011. The essential role of clathrin-mediated endocytosis in the infectious entry of human enterovirus 71. J. Biol. Chem. 286:309–321.
26. Lin YW, Lin HY, Tsou YL, Chitra E, Hsiao KN, Shao HY, Liu CC, Sia C, Chong P, Chow YH. 2012. Human SCARB2-mediated entry and endocytosis of EV71. PLoS One 7:e30507. doi:10.1371/journal.pone.0030507.
27. Sako D, Chang XJ, Barone KM, Vachino G, White HM, Shaw G, Veldman GM, Bean KM, Ahern TJ, Furie B, Cumming DA, Larsen GR. 1993. Expression cloning of a functional glycoprotein ligand for P-selectin. Cell 75:1179–1186.
28. Laszik Z, Jansen PJ, Cummings RD, Tedder TF, McEver RP, Moore KL. 1996. P-selectin glycoprotein ligand-1 is broadly expressed in cells of myeloid, lymphoid, and dendritic lineage and in some nonhematopoietic cells. Blood 88:3010–3021.
29. Somers WS, Tang J, Shaw GD, Camphausen RT. 2000. Insights into the molecular basis of leukocyte tethering and rolling revealed by structures of P- and E-selectin bound to SLe(X) and PSGL-1. Cell 103:467–479.
30. Ley K, Kansas GS. 2004. Selectins in T-cell recruitment to non-lymphoid tissues and sites of inflammation. Nat. Rev. Immunol. 4:325–335.
31. Nishimura Y, Wakita T, Shimizu H. 2010. Tyrosine sulfation of the amino terminus of PSGL-1 is critical for enterovirus 71 infection. PLoS Pathog. 6:e1001174. doi:10.1371/journal.ppat.1001174.
32. Liu J, Dong W, Quan X, Ma C, Qin C, Zhang L. 2012. Transgenic expression of human P-selectin glycoprotein ligand-1 is not sufficient for enterovirus 71 infection in mice. Arch. Virol. 157:539–543.
33. Bergelson JM. 2010. Receptors, p 73–86. *In* Ehrenfeld E, Domingo E, Roos RP (ed), The picornaviruses. ASM Press, Washington, DC.
34. Tuthill TJ, Groppelli E, Hogle JM, Rowlands DJ. 2010. Picornaviruses. Curr. Top. Microbiol. Immunol. 343:43–89.
35. Mendelsohn CL, Wimmer E, Racaniello VR. 1989. Cellular receptor for poliovirus: molecular cloning, nucleotide sequence, and expression of a new member of the immunoglobulin superfamily. Cell 56:855–865.
36. Koike S, Horie H, Ise I, Okitsu A, Yoshida M, Iizuka N, Takeuchi K, Takegami T, Nomoto A. 1990. The poliovirus receptor protein is produced both as membrane-bound and secreted forms. EMBO J. 9:3217–3224.
37. Staunton DE, Merluzzi VJ, Rothlein R, Barton R, Marlin SD, Springer TA. 1989. A cell adhesion molecule, ICAM-1, is the major surface receptor for rhinoviruses. Cell 56:849–853.
38. Tomassini JE, Graham D, DeWitt CM, Lineberger DW, Rodkey JA, Colonno RJ. 1989. cDNA cloning reveals that the major group rhinovirus receptor on HeLa cells is intercellular adhesion molecule 1. Proc. Natl. Acad. Sci. U. S. A. 86:4907–4911.
39. Greve JM, Davis G, Meyer AM, Forte CP, Yost SC, Marlor CW, Kamarck ME, McClelland A. 1989. The major human rhinovirus receptor is ICAM-1. Cell 56:839–847.
40. Duque H, Baxt B. 2003. Foot-and-mouth disease virus receptors: comparison of bovine alpha(V) integrin utilization by type A and O viruses. J. Virol. 77:2500–2511.
41. Hofer F, Gruenberger M, Kowalski H, Machat H, Huettinger M, Kuechler E, Blaas D. 1994. Members of the low density lipoprotein receptor family mediate cell entry of a minor-group common cold virus. Proc. Natl. Acad. Sci. U. S. A. 91:1839–1842.
42. Bergelson JM, Cunningham JA, Droguett G, Kurt-Jones EA, Krithivas A, Hong JS, Horwitz MS, Crowell RL, Finberg RW. 1997. Isolation of a common receptor for coxsackie B viruses and adenoviruses 2 and 5. Science 275:1320–1323.
43. Tomko RP, Xu R, Philipson L. 1997. HCAR and MCAR: the human and mouse cellular receptors for subgroup C adenoviruses and group B coxsackieviruses. Proc. Natl. Acad. Sci. U. S. A. 94:3352–3356.
44. Shafren DR, Bates RC, Agrez MV, Herd RL, Burns GF, Barry RD. 1995. Coxsackieviruses B1, B3, and B5 use decay accelerating factor as a receptor for cell attachment. J. Virol. 69:3873–3877.
45. Shafren DR, Williams DT, Barry RD. 1997. A decay-accelerating factor-binding strain of coxsackievirus B3 requires the coxsackievirus-adenovirus receptor protein to mediate lytic infection of rhabdomyosarcoma cells. J. Virol. 71:9844–9848.
46. Milstone AM, Petrella J, Sanchez MD, Mahmud M, Whitbeck JC, Bergelson JM. 2005. Interaction with coxsackievirus and adenovirus receptor, but not with decay-accelerating factor (DAF), induces A-particle formation in a DAF-binding coxsackievirus B3 isolate. J. Virol. 79:655–660.
47. Coyne CB, Bergelson JM. 2006. Virus-induced Abl and Fyn kinase signals permit coxsackievirus entry through epithelial tight junctions. Cell 124: 119–131.
48. Arita M, Koike S, Aoki J, Horie H, Nomoto A. 1998. Interaction of poliovirus with its purified receptor and conformational alteration in the virion. J. Virol. 72:3578–3586.
49. Fricks CE, Hogle JM. 1990. Cell-induced conformational change in poliovirus: externalization of the amino terminus of VP1 is responsible for liposome binding. J. Virol. 64:1934–1945.
50. Prchla E, Kuechler E, Blaas D, Fuchs R. 1994. Uncoating of human rhinovirus serotype 2 from late endosomes. J. Virol. 68:3713–3723.
51. Curry S, Abrams CC, Fry E, Crowther JC, Belsham GJ, Stuart DI, King AM. 1995. Viral RNA modulates the acid sensitivity of foot-and-mouth disease virus capsids. J. Virol. 69:430–438.
52. Tuthill TJ, Harlos K, Walter TS, Knowles NJ, Groppelli E, Rowlands DJ, Stuart DI, Fry EE. 2009. Equine rhinitis A virus and its low pH empty particle: clues towards an aphthovirus entry mechanism? PLoS Pathog. 5:e1000620. doi:10.1371/journal.ppat.1000620.
53. Nurani G, Lindqvist B, Casasnovas JM. 2003. Receptor priming of major group human rhinoviruses for uncoating and entry at mild low-pH environments. J. Virol. 77:11985–11991.
54. Nagata N, Shimizu H, Ami Y, Tano Y, Harashima A, Suzaki Y, Sato Y, Miyamura T, Sata T, Iwasaki T. 2002. Pyramidal and extrapyramidal involvement in experimental infection of cynomolgus monkeys with enterovirus 71. J. Med. Virol. 67:207–216.
55. Shiroki K, Kato H, Koike S, Odaka T, Nomoto A. 1993. Temperature-sensitive mouse cell factors for strand-specific initiation of poliovirus RNA synthesis. J. Virol. 67:3989–3996.
56. Hatakeyama S, Sakai-Tagawa Y, Kiso M, Goto H, Kawakami C, Mitamura K, Sugaya N, Suzuki Y, Kawaoka Y. 2005. Enhanced expression of an alpha2,6-linked sialic acid on MDCK cells improves isolation of human influenza viruses and evaluation of their sensitivity to a neuraminidase inhibitor. J. Clin. Microbiol. 43:4139–4146.
57. Yamayoshi S, Noda T, Ebihara H, Goto H, Morikawa Y, Lukashevich IS, Neumann G, Feldmann H, Kawaoka Y. 2008. Ebola virus matrix protein VP40 uses the COPII transport system for its intracellular transport. Cell Host Microbe 3:168–177.
58. Reed LJ, Muench H. 1938. A simple method of estimating fifty per cent endpoints. Am. J. Hyg. 27:493–499.
59. Arita M, Takebe Y, Wakita T, Shimizu H. 2010. A bifunctional anti-enterovirus compound that inhibits replication and the early stage of enterovirus 71 infection. J. Gen. Virol. 91:2734–2744.

60. **Dierssen U, Rehren F, Henke-Gendo C, Harste G, Heim A.** 2008. Rapid routine detection of enterovirus RNA in cerebrospinal fluid by a one-step real-time RT-PCR assay. J. Clin. Virol. **42**:58–64.
61. **Kaplan G, Freistadt MS, Racaniello VR.** 1990. Neutralization of poliovirus by cell receptors expressed in insect cells. J. Virol. **64**:4697–4702.
62. **Liu CC, Guo MS, Lin FH, Hsiao KN, Chang KH, Chou AH, Wang YC, Chen YC, Yang CS, Chong PC.** 2011. Purification and characterization of enterovirus 71 viral particles produced from Vero cells grown in a serum-free microcarrier bioreactor system. PLoS One **6**:e20005. doi:10.1371/journal.pone.0020005.
63. **Miyamura K, Nishimura Y, Abo M, Wakita T, Shimizu H.** 2011. Adaptive mutations in the genomes of enterovirus 71 strains following infection of mouse cells expressing human P-selectin glycoprotein ligand-1. J. Gen. Virol. **92**:287–291.
64. **Garriga D, Pickl-Herk A, Luque D, Wruss J, Caston JR, Blaas D, Verdaguer N.** 2012. Insights into minor group rhinovirus uncoating: the X-ray structure of the HRV2 empty capsid. PLoS Pathog. **8**:e1002473. doi:10.1371/journal.ppat.1002473.
65. **Bostina M, Levy H, Filman DJ, Hogle JM.** 2011. Poliovirus RNA is released from the capsid near a twofold symmetry axis. J. Virol. **85**:776–783.
66. **Lin TY, Hsia SH, Huang YC, Wu CT, Chang LY.** 2003. Proinflammatory cytokine reactions in enterovirus 71 infections of the central nervous system. Clin. Infect. Dis. **36**:269–274.
67. **Wang SM, Lei HY, Huang KJ, Wu JM, Wang JR, Yu CK, Su IJ, Liu CC.** 2003. Pathogenesis of enterovirus 71 brainstem encephalitis in pediatric patients: roles of cytokines and cellular immune activation in patients with pulmonary edema. J. Infect. Dis. **188**:564–570.

JVI
Journals.ASM.org

Quantification of the Dynamics of Enterovirus 71 Infection by Experimental-Mathematical Investigation

Mitsuko Fukuhara,[a,b] Shingo Iwami,[e,f,g,b,c] Kei Sato,[b,d] Yorihiro Nishimura,[h] Hiroyuki Shimizu,[h] Kazuyuki Aihara,[i,j] Yoshio Koyanagi[b,d]

Graduate School of Biostudies,[a] Laboratory of Viral Pathogenesis,[b] Laboratory of Primate Model,[c] and Center for Emerging Virus Research, Institute for Virus Research,[d] Kyoto University, Kyoto, Japan; Department of Biology, Faculty of Sciences, Kyushu University, Fukuoka, Japan[e]; Precursory Research for Embryonic Science and Technology (PRESTO), Japan Science and Technology Agency (JST), Kawaguchi, Saitama, Japan[f]; Graduate School of Mathematical Sciences, The University of Tokyo, Meguro-ku, Tokyo, Japan[g]; Department of Virology II, National Institute of Infectious Diseases, Musashimurayama, Tokyo, Japan[h]; Institute of Industrial Science[i] and Graduate School of Information Science and Technology,[j] The University of Tokyo, Meguro-ku, Tokyo, Japan

Enterovirus 71 (EV71) is the causative agent of hand-foot-and-mouth disease and can trigger neurological disorders. EV71 outbreaks are a major public health concern in Asia-Pacific countries. By performing experimental-mathematical investigation, we demonstrate here that viral productivity and transmissibility but not viral cytotoxicity are drastically different among EV71 strains and can be associated with their epidemiological backgrounds. This is the first report demonstrating the dynamics of nonenveloped virus replication in cell culture using mathematical modeling.

Human enteroviruses are nonenveloped viruses with a single-stranded positive-sense RNA genome that belong to the family *Picornaviridae* (1, 2). Enterovirus 71 (EV71) is one of the human enteroviruses and was first described in 1974 (3). It is well known that EV71 is the major causative agent of hand-foot-and-mouth disease (HFMD), a common febrile disease occurring mainly in infants and young children (1, 4). Although HFMD is usually self-limiting, EV71 infection can result in neurological disorders such as aseptic meningitis, flaccid paralysis, and fatal encephalitis (1, 4). However, there are no specific therapies for severe EV71 infections.

EV71 can be transmitted through the fecal-oral and respiratory routes (1). Since the 1970s, EV71 outbreaks have been periodically reported throughout the world (4, 5). In particular, since the late 1990s, severe EV71 outbreaks have occurred frequently in several countries in the Asia-Pacific region, including Taiwan, mainland China, Malaysia, and Vietnam, and are among the major concerns in the fields of epidemiology and public health in these countries (4, 5).

The dynamics of virus replication is complex because this event is composed of the all-at-once creation and destruction of infected cells along with virus propagation. Mathematical analysis is one of the most powerful approaches used to reveal the complicated events in the viral life cycle. By applying mathematical analysis to experimental data, we are able to quantitatively understand the dynamics of virus replication as estimated numerical parameters such as the half-life of infected cells ($\log 2/\delta$), the burst size of infectious viruses (p/δ; the net amount of virions produced by a cell during its lifetime), and the basic reproductive number ($R_0 = p\beta T_{max}/\delta c$; the number of cells newly infected by an infected cell). These parameters may provide novel insights into the dynamics of virus replication that cannot be addressed by conventional experimental techniques. So far, mathematical models have been used to study the replication dynamics of enveloped viruses such as human immunodeficiency virus type 1 (HIV-1) (6–8) and influenza virus (9–12) in *in vitro* cell culture. In order to obtain robust and reliable results by mathematical analysis, high-quality time course data are needed. Although some mathematical models of nonenveloped viruses focusing on viral replication kinetics in an infected cell have been reported (13–15), there is no report of the use of mathematical modeling and experimental data for the investigation of the dynamics of nonenveloped virus infection in cell culture.

To quantitatively elucidate the dynamics of EV71 replication, we first estimated the growth kinetics of RD cells, which have been commonly used for EV71 studies (16), under normal (i.e., mock-infected) conditions (Fig. 1A). To estimate viral growth kinetics in cell culture, we used the following mathematical model:

$$\frac{dT(t)}{dt} = gT(t)\left(1 - \frac{T(t)}{T_{max}}\right) \quad (1)$$

where the variable $T(t)$ is the number of RD cells at time t and the parameters g and T_{max} are the growth rate of RD cells (i.e., $\log 2/g$ is the doubling time) and the carrying capacity of a 12-well plate, respectively. Nonlinear least-squares regression (FindMinimum package of Mathematica 8.0) was performed to fit the model of equation 1 to the time course of the number of RD cells under normal conditions, yielding values of $g = 1.58 \pm 0.11$/day (doubling time of $\log 2/g = 10.57 \pm 0.69$ h) and $T_{max} = 1.18 \pm 0.11 \times 10^6$ cells/ml.

In this study, three representative strains of EV71, 1095 (17, 18), KED005 (19), and 02363 (20), that were isolated from HFMD patients with different epidemiological backgrounds were used (Table 1). For virus preparation and titration, we performed the following procedures. The virus solutions were prepared by using RD cells as previously described (21, 22). Infectivity was quantified by using RD cells and was calculated by the Kärber method

Received 10 June 2012 **Accepted** 16 October 2012
Published ahead of print 24 October 2012
Address correspondence to Shingo Iwami, siwami@kyushu-u.org, or Kei Sato, ksato@virus.kyoto-u.ac.jp.
M.F, S.I., and K.S. contributed equally to this study.

doi:10.1128/JVI.01453-12

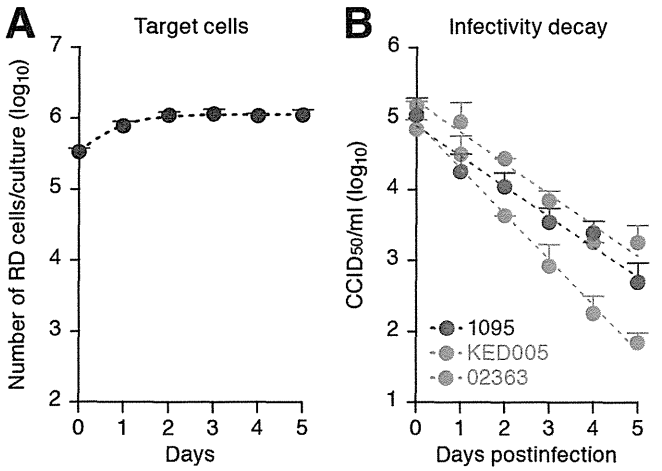

FIG 1 Dynamics of RD cell growth and decay of EV71 infectivity. (A) Growth kinetics of RD cells. Two hundred thousand RD cells in 1 ml of culture medium (Dulbecco's modified Eagle medium containing 10% fetal calf serum and antibiotics) were seeded into the wells of a 12-well plate. By harvesting the cells daily for 5 days, the growth kinetics of RD cells under this condition was estimated as described in the text. The estimated numerical values are g = 1.58 ± 0.11/day and T_{max} = 1.18 × 10^6 ± 0.11 × 10^6 cells/ml. (B) Decay of EV71 infectivity. One million $CCID_{50}$ of the three strains of EV71 solution in 1 ml of culture medium in the wells of a 12-well plate were incubated in an incubator (5% CO_2 and 37°C). The incubated virus solutions were harvested daily for 5 days, and the infectivity of the incubated virus solution, $V(t)$, was titrated as described in the text. The estimated numerical values are c = 1.01 ± 0.16, 1.46 ± 0.16, and 0.99 ± 0.08/day for strains 02363, KED005, and 1095, respectively. These assays were performed in triplicate. The average experimental data are shown as dots with standard deviations represented by bars, and the best fit of the mathematical model is shown as a broken line.

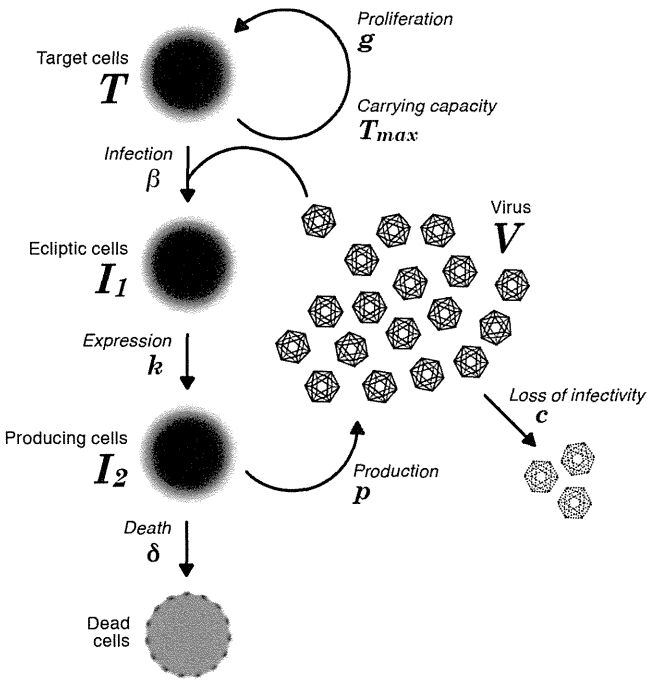

FIG 2 Schematic of our mathematical model. The variables $T(t)$, $I_1(t)$, and $I_2(t)$ are the numbers of target cells, ecliptic cells, and virus-producing cells, respectively, and $V(t)$ is viral infectivity. The parameters, k, δ, and β represent the rate of viral protein expression after infection, the rate of virus-producing cell death, and the rate constant of target cell infection by virus per day, respectively. It is assumed that infected cells release virus particles at a rate of p and that these virus particles lose their infectivity at a rate of c per day.

and expressed in 50% cell culture infective doses ($CCID_{50}$) as previously described (21–23).

Then we estimated the infectivity decay, c, of each virus strain under cell culture conditions (Fig. 1B). By performing a linear regression analysis that fits $\log V(t) = \log V(0) - ct$ to those data, the half-life of EV71 infectivity (log2/c) was calculated. Although the infectivity half-life of strain 1095 (16.53 ± 1.71 h) was comparable to that of strain 02363 (16.81 ± 2.98 h; P = 0.98 by Student's t test), the infectivity half-life of strain KED005 (11.52 ± 1.34 h) was significantly different from those of strains 1095 (P = 0.0084 by Student's t test) and 02363 (P = 0.049 by Student's t test). These results suggest that these EV71 strains differ in stability. In this regard, we found that 11 amino acid residues of the viral capsid proteins of the three EV71 strains used are different (data not shown). In fact, it has been suggested that the stability of poliovirus, a well-studied virus belonging to the family *Picornaviridae*, is determined by the amino acid sequences and/or conformations of viral capsid proteins VP1, VP2, VP3, and VP4 (24, 25). Therefore, it would be reasonable to assume that the difference in the decay of viral infectivity is due to the stability of infectious viral particles, which is influenced by the sequences and/or conformations of viral capsid proteins. Moreover, EV71 infection of humans occurs through the fecal-oral and respiratory routes (5). Our results suggest that EV71 stability may result in the survival of infectious viruses in the environment, which can be associated with the efficiency of EV71 spread in the human community.

TABLE 1 Three EV71 strains used in this study

Strain	Subgenogroup	Major symptom	Location	Yr	Accession no.
1095	C2	HFMD	Japan	1997	AB550332
KED005	C1	HFMD	Malaysia	1997	AB550340
02363	C1	HFMD	Thailand	2002	AB115495

In order to apply mathematical analyses robustly, we performed a time course infection experiment with RD cells (Fig. 2 and 3). To describe the *in vitro* kinetics of EV71 replication in our experimental system, we used a basic mathematical model with an eclipse phase of infection (i.e., the non-virus-producing period) as infection proceeds for analyzing viral kinetics (26, 27). Our model is defined by the equations

$$\frac{dT(t)}{dt} = gT(t)\left(1 - \frac{T(t)}{T_{max}}\right) - \beta T(t)V(t) \quad (2)$$

$$\frac{dI_1(t)}{dt} = \beta T(t)V(t) - kI_1(t) \quad (3)$$

$$\frac{I_2(t)}{dt} = kI_1(t) - \delta I_2(t) \quad (4)$$

$$\frac{dV(t)}{dt} = pI_2(t) - cV(t) \quad (5)$$

where $T(t)$, $I_1(t)$, and $I_1(t)$ are the numbers of target cells, ecliptic cells, and virus-producing cells per milliliter of culture, respectively, and $V(t)$ is viral infectivity measured the number of $CCID_{50}$ per milliliter of culture supernatant. The parameters k, δ, and β

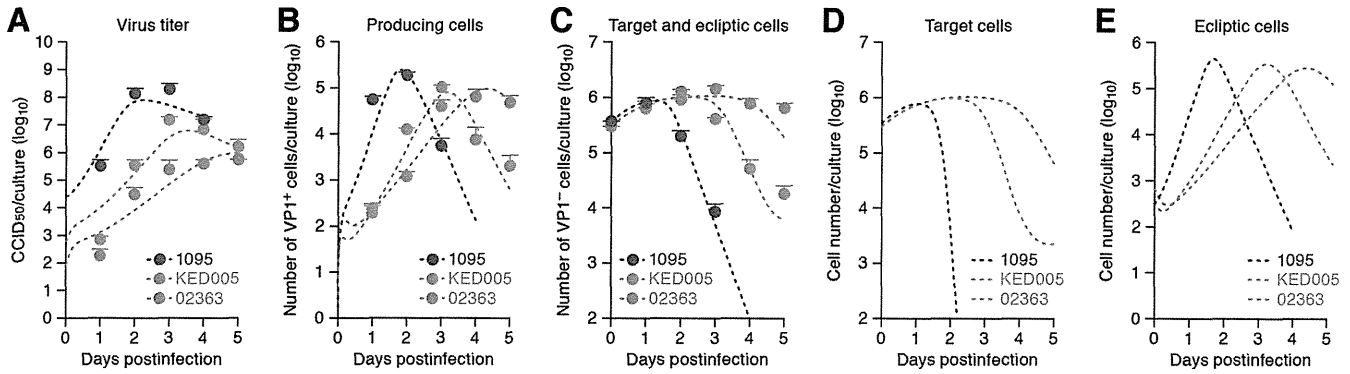

FIG 3 Dynamics of EV71 replication in RD cells. As described in the legend to Fig. 1, 2×10^5 RD cells were seeded 1 day prior to infection and the cells were counted just before infection. The cells were inoculated with EV71 at a multiplicity of infection of 0.01 in 0.5 ml of culture medium in an incubator (5% CO_2 and 37°C). At 1 h postinoculation, the culture supernatant was replaced with 1 ml of fresh culture medium. The cells and culture supernatants were harvested daily for 5 days. The virus infectivity in the culture supernatant was titrated as described in the text, and the harvested cells were counted. The cells were then used for flow cytometry according to the following procedure. The cells were permeabilized with Cytoperm/Cytofix solution (BD Biosciences) according to the manufacture's protocol and stained with a mouse anti-VP1 monoclonal antibody (clone MA105) labeled with Alexa Fluor 488 (22). The number of cells positive for the VP1 antigen was determined by using a FACSCalibur (BD Biosciences), and the numbers of VP1-positive cells (i.e., virus-producing cells) and VP1-negative cells at each time point were calculated. (A to C) The virus infectivity in the culture supernatant (A), the number of VP1-positive cells (virus-producing cells) in the culture (B), and the number of VP1-negative cells (target cells and ecliptic cells) in the culture (C), respectively, are shown. (D and E) Mathematical predictions of the kinetics of target cells in the culture (D) and ecliptic cells in the culture (E), respectively, are shown. These assays were performed in triplicate. In panels A to C, the average experimental data are shown as dots with standard deviations indicated by bars. In panels A to E, the best fit of the mathematical model is shown as a broken line.

represent the rate of VP1 protein expression after virus infection, the death rate of virus-producing cells, and the rate constant for infection of target cells by virus per day, respectively. In addition, we assumed that each infected cell releases p virus particle per day and that those progeny virus particles lose their infectivity at a rate of c per day. A schematic of our mathematical model is shown in Fig. 2.

We simultaneously fitted equations 2 to 5 to the concentrations of VP1-negative and VP1-positive RD cells and the level of viral infectivity in the culture supernatant ($CCID_{50}$) by using nonlinear least-squares regression, which minimizes the objective function

$$SSR = \sum_{i=1}^{6} \{log[T(t_i) + I_1(t_i)] - log N^e(t_i)\}^2 + \sum_{i=1}^{6} \{log I_2(t_i) - log I_2{}^e(t_i)\}^2 + \sum_{i=1}^{6} \{log V(t_i) - log V^e(t_i)\}^2 \quad (6)$$

where $T(t_i) + I_1(t)$, $I_2(t)$, and $V(t)$ are the values predicted by the model for viral-protein-negative cells, viral-protein-positive cells, and viral infectivity, given by the solution of equations 2 to 5 at measurement time t_i ($t_i = 0,\ldots, 4$ days for strain 1095 or $0,\ldots, 5$ days for strains KED005 and 02363). The variables with a superscript e are the corresponding experimental measurements of those quantities [$N^e(t_i)$ represents the concentration of VP1-negative RD cells in our experiment]. Here we note that g and T_{max} were estimated to be 1.58 per day and 1.18×10^6 cells per ml of medium from RD cell growth experiments, respectively (Fig. 1A), and k was assumed to be 4.0 per day (i.e., the delay prior to expression of VP1 is 6 h) in the fitting. In addition, we used c values of 1.01, 1.46, and 0.99/day for strains 02363, KED005, and 1095, respectively (Fig. 1B). The remaining three parameters (β, δ, and p), along with two initial values for $I_1(0)$ and $V(0)$ [$T(0) = 3.0 \times 10^5$ for strains 02363 and KED005, $T(0) = 3.7 \times 10^5$ for strain 1095, and $I_2(0) = 0$ for all strains were fixed], were determined by fitting the model to the data. The estimated parameters of the model and derived quantities are given in Table 2. Here the estimated initial values are $I_1(0) = 67.2 \pm 116.4$, 155.3 ± 37.8, and 830.9 ± 744.3 cells/ml and $V(0) = 582.5 \pm 298.8$, $1{,}979.8 \pm 1{,}061.8$, and $2{,}674.5 \pm 4{,}559.0$ $CCID_{50}$/ml for strains 02363, KED005, and 1095, respectively.

As summarized in Table 2, the half-life of virus-producing cells, log2/δ, which reflects the viral cytopathic potential, seemed to be different among the three strains examined. Since the three strains were isolated from patients with HFMD (17, 19, 20), which is a common and mild EV71-associated disease, the possibility that the viruses used in this study are relatively less pathogenic should be considered. However, one previous study demonstrated that strain 1095 caused neurological disorders such as flaccid paralysis, tremor, and ataxia in infected cynomolgus monkeys (21), which suggests that the severity of the EV71-associated diseases in

TABLE 2 Parameters estimated by mathematical-experimental analysis

Strain	Parameters				Derived quantities		
	β (10^{-6} $CCID_{50}$/ml · day^{-1})	p ($CCID_{50}$/day)	δ (day^{-1})	c (day^{-1})	Log2/δ (days)	p/δ ($CCID_{50}$)	R_0
1095	0.30 ± 0.11[a]	738.9 ± 153.3	6.22 ± 0.13	0.99 ± 0.08	2.67 ± 0.06	118.82 ± 25.1	37.35 ± 8.99
KED005	1.41 ± 0.15	146.8 ± 28.2	19.8 ± 3.90	1.46 ± 0.16	0.86 ± 0.16	7.43 ± 0.38	8.37 ± 0.82
02363	5.14 ± 1.02	13.4 ± 5.0	11.41 ± 1.50	1.01 ± 0.16	1.47 ± 0.19	1.16 ± 0.27	6.75 ± 0.16

[a] Values are averages and standard deviations.

the patients infected with the isolated virus cannot be directly represented by the apparent virulence of the corresponding EV71 isolates. In addition, a growing number of molecular epidemiological studies suggest that there is no correlation between the severity of clinical outcomes and specific genotypes of EV71 (28). Furthermore, it is well known that younger age is one of the major risk factors associated with severe EV71 infection (5). Therefore, host factors such as immunity level, viral susceptibility, and immunopathogenicity should also be considered when estimating the severity of EV71 infection. Taken together, the findings suggest that it is conceivable that the pathogenesis caused by EV71 infection in individuals is not only determined by the viral factors of EV71 strains, which are estimated by mathematical analyses through cell culture experiments *in vitro* and the genotypes of EV71 isolates, but is also associated with host factors.

On the other hand, the burst size (p/δ) and the basic reproductive number (R_0), which, respectively, represent the potentials of viral productivity and viral transmissibility, were drastically different in each strain compared to the difference in log2/δ (Table 2). In particular, these values of strain KED005 were significantly different from those of strain 02363, although the two viruses belong to the same subgenogroup (C1) (22). These findings suggest that a virus's productivity and transmissibility are not determined by its subgenogroup, which is based on the sequence of the VP1 region. In addition, it should be noted that the burst size and the basic reproductive number of strain 02363 were significantly lower than those of strains 1095 and KED005. It is noteworthy that strain 02363 was isolated from a sporadic patient with HFMD in Thailand in 2002 (20), while strains 1095 and KED005 were, respectively, isolated from HFMD patients during the large outbreaks in 1997 in Japan (17, 19) and Malaysia (19). However, the viral phenotypes and genotypes of EV71 remain to be clarified by using more EV71 strains with different genotypes and/or different epidemiological backgrounds. Taken together, these findings suggest that the burst size and the basic reproductive number of each EV71 strain are novel criteria exhibiting viral characteristics that can correlate with the epidemiological backgrounds of EV71 infection. In fact, Mitchell et al. have recently performed mathematical and computational modeling to quantify the replication kinetics of three different types of influenza virus (H5N1 avian influenza virus, H1N1 seasonal influenza virus, and H1N1 pandemic influenza virus that emerged in 2009) (10). In that study, the authors suggested that the basic reproductive number of each influenza virus in *in vitro* cell culture correlates with the efficiency of person-to-person virus transmission (10). Therefore, it would be reasonable to assume that derived quantities of viral infection such as p/δ and R_0 can represent the different epidemic potentials of viruses, which could not be addressed in previous experiments by using conventional viral phenotypic markers.

In summary, we first demonstrated that novel EV71 phenotypes, the burst size and the basic reproductive number, that are estimated by our experimental-mathematical analyses could be associated with the rate of infection and transmissibility of viruses in the community. As mentioned above, EV71 outbreaks are a major concern in the Asia-Pacific region (4). Our strategy will be one of the informative approaches to estimate the epidemic potential of EV71 and will provide novel insights into the field of EV71 epidemiology in these countries. Moreover, this is the first demonstration that our mathematical modeling can be used to quantify the kinetics of not only enveloped viruses (e.g., HIV-1 and influenza virus) but also nonenveloped viruses, including EV71. The synergistic experimental-mathematical strategy is a powerful methodology and will be used to quantitatively investigate the dynamics of virus infections in a way that is not possible by conventional experimental strategies.

ACKNOWLEDGMENTS

We thank Naoko Misawa (Laboratory of Viral Pathogenesis, Institute for Virus Research, Kyoto University) for her generous help with this study.

This research was supported in part by the following: Research on Emerging and Re-emerging Infectious Diseases (to Y.N., H.S., and Y.K.) from the Ministry of Health, Labor and Welfare of Japan; Grant-in-Aid for Young Scientists B23790500 (to K.S.) and Grant-in-Aid for Scientific Research B22390092 (to H.S.) from the Japan Society for the Promotion of Science (JSPS); the Uehara Memorial Foundation (to K.S.); the Shimizu Foundation for Immunological Research Grant (to K.S.); the JST PRESTO program (to S.I.); and the Aihara Innovative Mathematical Modeling Project, JSPS, through the Funding Program for World-Leading Innovative R & D on Science and Technology (FIRST program), initiated by the Council for Science and Technology Policy (to S.I., K.S., and K.A.).

REFERENCES

1. **Pallansch M, Roos R.** 2007. Enteroviruses: polioviruses, coxsackieviruses, echoviruses, and newer enteroviruses, p 839–893. *In* D. M. Knipe and P. M. Howley (ed), Fields virology, 5th ed, vol 2. Lippincott Williams & Wilkins, Philadelphia, PA.
2. **Racaniello VR.** 2007. Picornaviridae: the viruses and their replication, p 795–838. *In* D. M. Knipe and P. M. Howley (ed), Fields virology, 5th ed, vol 2. Lippincott Williams & Wilkins, Philadelphia, PA.
3. **Schmidt NJ, Lennette EH, Ho HH.** 1974. An apparently new enterovirus isolated from patients with disease of the central nervous system. J. Infect. Dis. **129**:304–309.
4. **World Health Organization.** 2011. A guide to clinical management and public health response for hand, hoot and mouth disease (HFMD). WHO Press, Geneva, Switzerland.
5. **Solomon T, Lewthwaite P, Perera D, Cardosa MJ, McMinn P, Ooi MH.** 2010. Virology, epidemiology, pathogenesis, and control of enterovirus 71. Lancet Infect. Dis. **10**:778–790.
6. **Dimitrov DS, Willey RL, Sato H, Chang LJ, Blumenthal R, Martin MA.** 1993. Quantitation of human immunodeficiency virus type 1 infection kinetics. J. Virol. **67**:2182–2190.
7. **Iwami S, Holder BP, Beauchemin CA, Morita S, Tada T, Sato K, Igarashi T, Miura T.** 2012. Quantification system for the viral dynamics of a highly pathogenic simian/human immunodeficiency virus based on an in vitro experiment and a mathematical model. Retrovirology **9**:18. doi:10.1186/1742-4690-9-18.
8. **Iwami S, Sato K, De Boer RJ, Aihara K, Miura T, Koyanagi Y.** 2012. Identifying viral parameters from in vitro cell cultures. Front. Microbiol. **3**:319.
9. **Beauchemin CA, McSharry JJ, Drusano GL, Nguyen JT, Went GT, Ribeiro RM, Perelson AS.** 2008. Modeling amantadine treatment of influenza A virus in vitro. J. Theor. Biol. **254**:439–451.
10. **Mitchell H, Levin D, Forrest S, Beauchemin CA, Tipper J, Knight J, Donart N, Layton RC, Pyles J, Gao P, Harrod KS, Perelson AS, Koster F.** 2011. Higher level of replication efficiency of 2009 (H1N1) pandemic influenza virus than those of seasonal and avian strains: kinetics from epithelial cell culture and computational modeling. J. Virol. **85**:1125–1135.
11. **Möhler L, Flockerzi D, Sann H, Reichl U.** 2005. Mathematical model of influenza A virus production in large-scale microcarrier culture. Biotechnol. Bioeng. **90**:46–58.
12. **Schulze-Horsel J, Schulze M, Agalaridis G, Genzel Y, Reichl U.** 2009. Infection dynamics and virus-induced apoptosis in cell culture-based influenza vaccine production—Flow cytometry and mathematical modeling. Vaccine **27**:2712–2722.
13. **Eigen M, Biebricher CK, Gebinoga M, Gardiner WC.** 1991. The hypercycle. Coupling of RNA and protein biosynthesis in the infection cycle of an RNA bacteriophage. Biochemistry **30**:11005–11018.

14. **Krakauer DC, Komarova NL.** 2003. Levels of selection in positive-strand virus dynamics. J. Evol. Biol. **16**:64–73.
15. **Regoes RR, Crotty S, Antia R, Tanaka MM.** 2005. Optimal replication of poliovirus within cells. Am. Nat. **165**:364–373.
16. **Yamayoshi S, Yamashita Y, Li J, Hanagata N, Minowa T, Takemura T, Koike S.** 2009. Scavenger receptor B2 is a cellular receptor for enterovirus 71. Nat. Med. **15**:798–801.
17. **Cardosa MJ, Perera D, Brown BA, Cheon D, Chan HM, Chan KP, Cho H, McMinn P.** 2003. Molecular epidemiology of human enterovirus 71 strains and recent outbreaks in the Asia-Pacific region: comparative analysis of the VP1 and VP4 genes. Emerg. Infect. Dis. **9**:461–468.
18. **Komatsu H, Shimizu Y, Takeuchi Y, Ishiko H, Takada H.** 1999. Outbreak of severe neurologic involvement associated with enterovirus 71 infection. Pediatr. Neurol. **20**:17–23.
19. **Shimizu H, Utama A, Yoshii K, Yoshida H, Yoneyama T, Sinniah M, Yusof MA, Okuno Y, Okabe N, Shih SR, Chen HY, Wang GR, Kao CL, Chang KS, Miyamura T, Hagiwara A.** 1999. Enterovirus 71 from fatal and nonfatal cases of hand, foot and mouth disease epidemics in Malaysia, Japan and Taiwan in 1997-1998. Jpn. J. Infect. Dis. **52**:12–15.
20. **Shimizu H, Utama A, Onnimala N, Li C, Li-Bi Z, Yu-Jie M, Pongsuwanna Y, Miyamura T.** 2004. Molecular epidemiology of enterovirus 71 infection in the western Pacific region. Pediatr. Int. **46**:231–235.
21. **Nagata N, Shimizu H, Ami Y, Tano Y, Harashima A, Suzaki Y, Sato Y, Miyamura T, Sata T, Iwasaki T.** 2002. Pyramidal and extrapyramidal involvement in experimental infection of cynomolgus monkeys with enterovirus 71. J. Med. Virol. **67**:207–216.
22. **Nishimura Y, Shimojima M, Tano Y, Miyamura T, Wakita T, Shimizu H.** 2009. Human P-selectin glycoprotein ligand-1 is a functional receptor for enterovirus 71. Nat. Med. **15**:794–797.
23. **World Health Organization.** 2004. Polio laboratory manual, 4th ed. WHO Document Production Services, Geneva, Switzerland.
24. **Moscufo N, Chow M.** 1992. Myristate-protein interactions in poliovirus: interactions of VP4 threonine 28 contribute to the structural conformation of assembly intermediates and the stability of assembled virions. J. Virol. **66**:6849–6857.
25. **Simons J, Rogove A, Moscufo N, Reynolds C, Chow M.** 1993. Efficient analysis of nonviable poliovirus capsid mutants. J. Virol. **67**:1734–1738.
26. **Nowak MA, May RM.** 2000. Virus dynamics: the mathematical foundations of immunology and virology. Oxford University Press, Oxford, United Kingdom.
27. **Perelson AS.** 2002. Modelling viral and immune system dynamics. Nat. Rev. Immunol. **2**:28–36.
28. **Chu PY, Lin KH, Hwang KP, Chou LC, Wang CF, Shih SR, Wang JR, Shimada Y, Ishiko H.** 2001. Molecular epidemiology of enterovirus 71 in Taiwan. Arch. Virol. **146**:589–600.

zjv00913/zjv7532d13z | xppws | S=1 | 2/21/13 | 11:41 | 4/C Fig: 1,3,4,7,8 | ArtID: 02954-12 | NLM: research-article | CE: CLD

Editor: Kirkegaard | Section: Genetic Diversity and Evolution | Designation: T

JVI Journals.ASM.org

Multiple Independent Emergences of Type 2 Vaccine-Derived Polioviruses during a Large Outbreak in Northern Nigeria

AQ: au Cara C. Burns,[a] Jing Shaw,[a] Jaume Jorba,[a] David Bukbuk,[c] Festus Adu,[d] Nicksy Gumede,[e] Muhammed Ali Pate,[f] Emmanuel Ade Abanida,[f] Alex Gasasira,[g] Jane Iber,[a] Qi Chen,[a] Annelet Vincent,[a] Paul Chenoweth,[b] Elizabeth Henderson,[a] Kathleen Wannemuehler,[b] Asif Naeem,[h] Rifqiyah Nur Umami,[h] Yorihiro Nishimura,[h] Hiroyuki Shimizu,[h] Marycelin Baba,[c] Adekunle Adeniji,[d] A. J. Williams,[a] David R. Kilpatrick,[a] M. Steven Oberste,[a] Steven G. Wassilak,[b] Oyewale Tomori,[i] Mark A. Pallansch,[a] Olen Kew[a]

Division of Viral Diseases, National Center for Immunization and Respiratory Diseases,[a] and Global Immunization Division, Center for Global Health,[b] Centers for Disease Control and Prevention, Atlanta, Georgia, USA; University of Maiduguri Teaching Hospital, Maiduguri,[c] and Department of Virology, College of Medicine, University of Ibadan, Ibadan,[d] Nigeria; Virology Division, National Institute of Communicable Diseases, Johannesburg, South Africa[e]; National Primary Health Care Development Agency,[f] and World Health Organization-Nigeria,[g] Abuja, Nigeria; Department of Virology II, National Institute of Infectious Diseases, Tokyo, Japan[h]; Redeemer's University, Redemption City, Ogun State, Nigeria[i]

AQ:A-C **Since 2005, a large poliomyelitis outbreak associated with type 2 circulating vaccine-derived poliovirus (cVDPV2) has occurred in northern Nigeria, where immunization coverage with trivalent oral poliovirus vaccine (tOPV) has been low. Phylogenetic analysis of P1/capsid region sequences of isolates from each of the 403 cases reported in 2005 to 2011 resolved the outbreak into 23 independent type 2 vaccine-derived poliovirus (VDPV2) emergences, at least 7 of which established circulating lineage groups. Virus from one emergence (lineage group 2005-8; 361 isolates) was estimated to have circulated for over 6 years. The population of the major cVDPV2 lineage group expanded rapidly in early 2009, fell sharply after two tOPV rounds in mid-2009, and gradually expanded again through 2011. The two major determinants of attenuation of the Sabin 2 oral poliovirus vaccine strain (A_{481} in the 5′-untranslated region [5′-UTR] and VP1-Ile_{143}) had been replaced in all VDPV2 isolates; most A_{481} 5′-UTR replacements occurred by recombination with other enteroviruses. cVDPV2 isolates representing different lineage groups had biological properties indistinguishable from those of wild polioviruses, including efficient growth in neuron-derived HEK293 cells, the capacity to cause paralytic disease in both humans and PVR-Tg21 transgenic mice, loss of the temperature-sensitive phenotype, and the capacity for sustained person-to-person transmission. We estimate from the poliomyelitis case count and the paralytic case-to-infection ratio for type 2 wild poliovirus infections that ~700,000 cVDPV2 infections have occurred during the outbreak. The detection of multiple concurrent cVDPV2 outbreaks in northern Nigeria highlights the risks of cVDPV emergence accompanying tOPV use at low rates of coverage in developing countries.**

AQ: D A major milestone for the World Health Organization (WHO) Global Polio Eradication Initiative has been the apparent eradication of indigenous wild poliovirus type 2 (WPV2), last detected in West Africa in the mid-1990s (F. Adu and C. Akoua-Koffi, unpublished data) and last detected worldwide in Uttar Pradesh, India, in 1999 (1). Key factors contributing to this achievement were the widespread use of supplemental immunization activities (SIAs) in the form of mass vaccination campaigns with oral poliovirus vaccine (OPV) (2), the high immunogenicity of the Sabin 2 OPV strain in trivalent OPV (tOPV) formulations (3), and the marked tendency of the Sabin 2 strain to spread to secondary contacts (4, 5), especially in settings with poor sanitation and high population densities (6).

Another important milestone has been the decline in WPV incidence in Nigeria, from 796 polio cases (719 WPV1 and 77 WPV3) reported in 2008 to 388 polio cases (75 WPV1 and 313 WPV3) reported in 2009 and 21 cases (8 WPV1 and 13 WPV3) reported in 2010 (7, 8). However, the reported number of WPV cases rose to 62 (47 WPV1 and 15 WPV3) in 2011 (for updates, see the Global Polio Eradication Initiative website [http://www.polioeradication.org/]), as immunization activities weakened in the northern states where polio is endemic (9). Until 2010, northern Nigeria had been an especially intense focus of WPV endemicity and the main exporter of WPV to countries in Africa and Asia (10–13). Key factors contributing to the decline in polio incidence have been the rising rates of OPV coverage in the SIAs following improved community engagement (8), the intensive use of monovalent OPV type 1 (mOPV1) starting in March 2006 and mOPV3 starting in July 2007 (14, 15), and continued sensitive acute flaccid paralysis (AFP) case surveillance linked to virologic surveillance to identify WPV reservoir communities (7, 8, 16). However, the emphasis on the use of mOPV1 and mOPV3 (and bivalent OPV [types 1 and 3] introduced in January 2010) (8, 17, 18) in SIAs to stop WPV transmission coupled with the persistently low rates of routine immunization coverage with tOPV have allowed a population immunity gap for poliovirus type 2 (PV2) to develop in northern Nigeria, leading to the emergence and spread of neurovirulent type 2 vaccine-derived poliovirus (VDPV2) (14, 15, 19–

Received 22 October 2012 **Accepted** 7 February 2013

Published ahead of print 13 February 2013

Address correspondence to Cara C. Burns, CBurns@cdc.gov.

This paper is dedicated to Walter Dowdle in recognition of his distinguished career of service to global public health.

Supplemental material for this article may be found at http://dx.doi.org/10.1128/JVI.02954-12.

doi:10.1128/JVI.02954-12

22). By 2005, all three poliovirus serotypes were again cocirculating in Nigeria, a condition not observed elsewhere during the preceding 6 years (1).

The principal biological mechanism underlying the emergence of VDPVs is the intrinsic genetic instability of the OPV strains, such that revertants with increased neurovirulence are selected for during replication of OPV in the human intestine (23). One clinical consequence of the genetic lability of OPV, the occurrence of cases of vaccine-associated paralytic poliomyelitis (VAPP) among OPV recipients and their close contacts (3), has been recognized for nearly 5 decades (24). The current worldwide incidence of VAPP is estimated to be 250 to 500 sporadically distributed cases per year (3). The serotype distribution of VAPP cases among immunologically healthy individuals is uneven: Sabin 1 is rarely implicated, Sabin 2 is most frequently associated with VAPP in unimmunized contacts of OPV recipients, and Sabin 3 is most frequently associated with VAPP in OPV recipients (25–27). Vaccine-related isolates from immunologically healthy VAPP patients typically show limited genetic divergence (<1% of nucleotide positions) from the parental OPV strains (apart from mosaic genomes arising from vaccine/vaccine recombination) (28, 29), consistent with durations of infections of only 1 to 2 months (30). Individuals with primary immunodeficiencies have an ~3,000-fold-higher risk of VAPP (31) and, in rare instances, the further risk of prolonged infection (some lasting >10 years) with excretion of highly divergent immunodeficiency-associated VDPVs (iVDPVs) (3, 19, 21, 22, 32–36).

Quite distinct from iVDPVs are the circulating VDPVs (cVDPVs), which can emerge and spread in settings of low type-specific population immunity (32). cVDPV outbreaks have occurred and have been controlled in Egypt (37), Hispaniola (Haiti and the Dominican Republic) (38), the Philippines (39), Madagascar (40, 41), Indonesia (42), Cambodia (20), Myanmar (20), and China (43, 44). Within the past 3 years, cVDPV outbreaks have emerged in the Democratic Republic of Congo (type 2, 2008 to 2012), Ethiopia (type 2, 2008 to 2009, and type 3, 2009 to 2010), Somalia (type 2, 2008 to 2011), India (type 2, 2009 to 2010), Afghanistan (type 2, 2010 to 2012), Mozambique (type 1, 2011), Yemen (type 2, 2011), Chad (type 2, 2012), and Pakistan (type 2, 2012) (19, 21, 22, 45) (for updates, see the Global Polio Eradication Initiative website [http://www.polioeradication.org/]). Most cVDPV outbreaks involve Sabin types 2 and 1, rarely type 3. In addition to the well-defined cVDPV and iVDPV categories, VDPV isolates may be assigned to a third category, ambiguous VDPVs (aVDPVs), when there is no clear evidence of community circulation or immunodeficiency (19, 22, 46).

VDPVs have been defined for the purposes of global poliovirus surveillance as having >1% nucleotide sequence divergence (i.e., ≥10 nucleotide [nt] substitutions) from their parental Sabin strains in the ~900-nt region encoding the major capsid protein, VP1 (16, 21, 32). This definition follows from the high rate of nucleotide sequence evolution in poliovirus (~1% per year) (47) and the normal period of poliovirus excretion of less than 3 months (30, 32). The demarcation for VDPV2s has recently been lowered to >0.6% nucleotide sequence divergence (i.e., ≥6 nt substitutions) in view of the findings presented in this report (22, 48) and similar findings in the Democratic Republic of Congo (22, 48).

Nigeria has recorded the largest VDPV outbreak in terms of the number of reported cases, with a total of 403 cases associated with VDPV2 infection reported during 2005 to 2011 (14, 15, 19–22, 49). Here we describe the basic genetic properties of and genetic relationships among Nigerian VDPV2 outbreak isolates obtained from July 2005 to December 2011 and present evidence that the outbreak was associated with 23 independent VDPV2 emergences, 7 of which expanded into well-defined cVDPV2 lineage groups and several others of which may have signaled more limited cVDPV2 transmission. We further describe the population dynamics of the major cVDPV2 lineage group during the outbreak and the key biological properties of selected VDPV2 isolates. Finally, we discuss the implications of multiple, concurrent cVDPV outbreaks for current and future strategies to secure the cessation of all poliovirus transmission.

MATERIALS AND METHODS

Virus isolation and identification. Viruses in stool specimens obtained from patients with AFP (see Table S1 in the supplemental material) were isolated in L20B (mouse L cells expressing the human CD155 poliovirus receptor [PVR]) (50, 51) and RD (human rhabdomyosarcoma cells; ATCC CCL-136) cell lines according to standard protocols (52). Isolates were characterized by reverse transcriptase PCR (RT-PCR) assays using enterovirus-specific and poliovirus group-, serotype-, and Sabin strain-specific primer sets (52–55) and enzyme-linked immunosorbent assays using highly specific cross-absorbed hyperimmune rabbit sera (52, 56). Since August 2006, vaccine-related poliovirus isolates have been screened for VDPVs by using a real-time RT-PCR assay (16, 48). VDPVs were identified by VP1 sequencing (37, 57).

Nucleic acid sequencing. RNA extraction and RT-PCR amplification and cycle sequencing were performed as previously described (37, 57). Terminal sequences of 17 VDPV2 isolate genomes (all but one from lineage group 2005-8) were determined by using 5′ rapid amplification of the cDNA ends (RACE) kits (Life Technologies) according to the manufacturer's instructions. The first 19 nt at the 5′ ends of the remaining genomes were derived from the primer, which matched the 17 identical terminal sequences determined by RACE. Numbering of nucleotide positions followed that described previously for Sabin 2 (58, 59).

Phylogenetic analysis. Sequence relationships (all nucleotide substitutions [K_T]) in the P1/capsid region (nt 748 to 3384) among all VDPV2 isolates were summarized in phylogenetic trees constructed by Bayesian Markov chain Monte Carlo (MCMC) analysis implemented in BEAST v. 1.7 (60). Two independent MCMC chains were run for each BEAST analysis (200 million generations each for lineage group 2005-8 and 50 million generations each for the other lineage groups). High-performance computing was achieved by integrating the BEAGLE library (61) into BEAST runs. Sampling efficiency was examined by measuring the integrated autocorrelation time and effective sample size, as implemented in TRACER (MCMC Trace Analysis Tool, v1.5 [http://tree.bio.ed.ac.uk/software/tracer/]). Substitution parameters were estimated from the data set. Codon deletions at VP1-Thr_{24} were treated as single-nucleotide substitutions. Hypothesis testing within nested models of evolution was performed by using MODELTEST (62). Maximum clade credibility (MCC) trees including all VDPV2 isolates and representatives of all VDPV2 emergences were rooted to the P1/capsid region sequences of Sabin 2 and scaled to time by assuming a strict molecular clock with a K_T substitution rate of 1.1×10^{-2} nt substitutions/site/year. Trees of individual lineage groups were constructed similarly, except that the root for lineage group 2005-8 was a simulated P1/capsid region sequence of a nonmutated S3/S2 recombinant homologue of the observed VDPV recombinants. Phylogenetic trees were displayed and edited by using FigTree (http://tree.bio.ed.ac.uk/software/figtree/).

A P1/capsid subtree including representative isolates from all lineages was inferred after two independent MCMC chains were run for 1 million generations each in Mr. Bayes (63), as implemented in the plug-in version for the Geneious v5.6 software package. AQ: E

Phylogenetic resolution of separate emergences. P1/capsid region sequences of isolates across and within emergences were compared in difference tables constructed by using MEGA5 software (64), with pairwise P1/capsid region nucleotide differences shown below the diagonal and the proportion of shared P1/capsid region nucleotide differences from Sabin 2 (excluding the codon for amino acid $VP1_{143}$) shown above the diagonal.

Estimation of dates of the initiating OPV doses. Dates of the tOPV doses that initiated each of the 23 observed emergences were estimated from K_T values for P1/capsid region sequences by using the Bayesian inference method reported previously by Shapiro et al. (65), implemented in BEAST under the assumption of a uniform K_T substitution rate of 1.1×10^{-2} nt substitutions/site/year. Mean estimated values and 95% highest posterior density (HPD) intervals for tOPV dose dates and inferred mean estimated times were calculated according to BEAST procedures, as described above.

Estimation of the number of lineages transiting the low-transmission season for poliovirus. The number of lineages that continued through the seasonal lows for poliovirus transmission in northern Nigeria from December to January was estimated from the topology of the Bayesian MCC trees of the 7 lineage groups and the estimated duration of replication of virus of the 16 other separate emergences. K_T substitution rates for lineage groups 2005-6, 2005-8, 2005-10, and 2007-4 were estimated from the data sets; otherwise, the rate was assumed to be 1.1×10^{-2} nt substitutions/site/year. A bifurcation of a branch in December was counted as two lineages, and one in January was counted as one lineage. Lineages whose last isolate was detected in January were not counted as transiting the low-transmission season. Long branches that spanned multiple years were counted across each seasonal low.

VDPV population dynamics during the outbreak. The demographic history of all Nigerian VDPV2s was estimated under the Bayesian skyline plot model (66), as implemented in BEAST. The distribution of mean and 95% HPD effective population size values (N_e) for 2005 to 2011 was analyzed in TRACER.

Phenotypic characterization of VDPV isolates. Phenotypic properties of representative isolates of each VDPV2 emergence were compared with those of Sabin 2 and MEF-1 (a neurovirulent WPV2 isolate whose robust growth favored its selection as the type 2 component of the inactivated poliovirus vaccine [IPV]) (67).

(i) Virus replication in HEK293 cells. Monolayers of HEK293 cells (human neuron-derived cells; ATCC CRL-1573) (68) were infected with virus at a multiplicity of infection (MOI) of 10 PFU/cell and incubated for 24 h at 37.0°C and 39.5°C, as described previously by Campbell et al. (69). Virus was liberated by two freeze-thaw cycles, and infectivity titers were measured by plaque assays on HeLa cell monolayers incubated at 37.0°C, as described previously (70).

(ii) Neurovirulence testing in PVR-Tg21 mice. Neurovirulence tests on VDPV2 isolates were carried out by using PVR-Tg21 (71) mice as previously described (39). The mice were purchased from the Central Laboratories for Experimental Animals (Kanagawa, Japan). The type 2 reference strains were Sabin 2 and MEF-1. Eight mice (equal numbers of males and females) were inoculated (30 μl/mouse) intracerebrally for each virus dilution (in 10-fold increments; range, 1.5 to 6.5 log 50% tissue culture infective doses [$TCID_{50}$]/mouse and up to 7.0 log $TCID_{50}$/mouse for Sabin 2). Mice were examined daily for 14 days postinoculation, and the times of paralysis or death were recorded. The virus titer that induced paralysis or death in 50% of inoculated mice (PD_{50}) was calculated according to the method of Kärber (72).

(iii) Virus infectivity yields at supraoptimal temperatures. Virus was grown to high titers in RD cell monolayers at 37.0°C, and infectivity yields were measured by plaque assays (70) on L20B cells incubated at 37.0°C and 39.5°C (73).

Nucleotide sequence accession numbers. P1/capsid region sequences of all Nigerian VDPV2 isolates described here, including complete genomic sequences of the first isolates of each emergence, were deposited in the GenBank database under accession numbers JX274980 to JX275382 (see Table S1 in the supplemental material).

RESULTS

Identification of VDPV2 isolates. The standard method for VDPV screening by the Global Polio Laboratory Network (GPLN) (52) has been to identify vaccine-related isolates by their genetic properties by using RT-PCR (55) (or other molecular methods) followed by antigenic characterization (74). Antigenic variants of the vaccine strains were flagged as candidate VDPVs (32) to be further characterized by sequencing of the VP1 capsid region (19). However, the early (2005-2006) VDPV2 isolates from Nigeria did not appear to be antigenic variants, such that the routine screening algorithm did not initially signal any VDPV emergence. An outbreak was first suspected in 2006 by the frequent isolation from AFP patients of vaccine-related PV2 (15), the serotype most frequently associated with cVDPV outbreaks (19, 21, 22, 32, 45), with temporal and geographic clustering in the northern states (Fig. 1). The higher isolation rate for PV2 appeared to be anomalous because WPV2 was believed to have been eradicated, many patients had no known exposure to tOPV, routine immunization coverage with tOPV was low, and only two of the six SIAs in 2006 used tOPV, as the remainder used mOPV1 (14, 15). Sequencing of the VP1 region identified most of the recent PV2 isolates from the north as VDPV2s (15). In recognition of the limitations of screening for VDPVs by antigenic methods, a new real-time RT-PCR assay was developed for VDPV screening (16, 19, 48) and applied retrospectively and prospectively to Nigerian PV2 isolates.

Range of VP1 sequence divergence among Sabin 2-related case isolates. During 2005 to 2011, 1,201 PV2s were isolated from individual AFP patients in Nigeria; all were related to Sabin 2. Of these, 695 (612 from the north and 83 from the south) were sequenced in the VP1 region. Most had been sequenced as candidate VDPV2s after screening by real-time RT-PCR, but isolates with <6 nt substitutions in VP1 had been sequenced independently of the screening assay results. The sequenced isolates diverged from Sabin 2 at 0 to 59 VP1 nucleotide positions (0% to 6.5%) (Fig. 2). Sabin 2-related isolates with ≥6 nt substitutions in the VP1 region are unusual and, on the basis of the findings reported here, have been redefined as VDPV2s (22, 48). Nearly all (401/403; 99.5%) of the VDPV2s detected were from cases in 15 northern states (Fig. 1 and 2A) (7, 15) known to have widening gaps of immunity to PV2 because of low routine immunization coverage with tOPV and a reduced frequency of SIAs with tOPV after 2005 (14, 15). Only two VDPV2 case isolates, of limited divergence (6 VP1 nucleotide substitutions), were found in the southern states (Fig. 1 and 2B). Among isolates with 0 to 5 VP1 nucleotide substitutions, in both the north and the south, the distribution of isolates showed a steep decline with increasing divergence from Sabin 2. However, in the north, the number of isolates with ≥6 nt substitutions increased (Fig. 2A). None of the Sabin 2-related isolates with ≤5 VP1 nucleotide substitutions appeared to be ancestral to any subsequent isolates. All isolates with a substitution in the VP1 region had a missense substitution within the codon for $VP1_{143}$, a result of strong selection against the Sabin 2 allele (see below). Isolates with no VP1 substitutions are underrepresented in Fig. 2 because they were not flagged for sequencing by the real-time RT-PCR screening assay, which targets substitutions in VP1.

The 403 VDPV2s isolated from AFP patients (1 isolate per patient; includes 1 isolate from a healthy contact of an AFP pa-

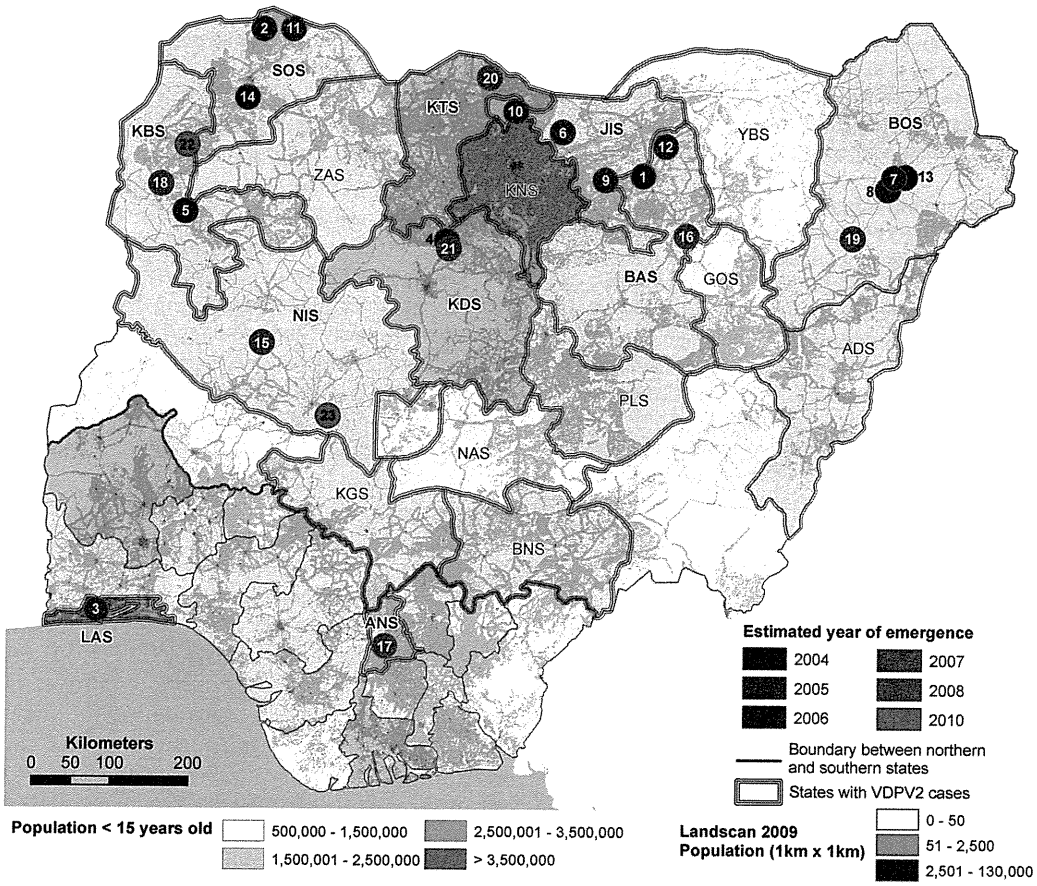

COLOR

AQ: K FIG 1 Map of Nigeria showing state boundaries, population density by LandScan (http://www.ornl.gov/landscan/), and location (circles color-coded by estimated year of emergence) of first acute flaccid paralysis (AFP) cases found to be associated with each independent type 2 vaccine-derived poliovirus (VDPV2) emergence. The numbers 1 to 23 correspond to emergences listed in Table 1 according to the order of the estimated date of the initiating tOPV dose. The bold red line indicates the boundary between the northern and southern states. Abbreviations for Nigerian states (S) with VDPV2 cases (14, 15) are as follows: ADS, Adamawa; ANS, Anambra; BAS, Bauchi; BNS, Benue; BOS, Borno; JIS, Jigawa; KBS, Kebbi; KDS, Kaduna; KNS, Kano; KTS, Katsina; KGS, Kogi; LAS, Lagos; NAS, Nasarawa; NIS, Niger; PLS, Plateau; SOS, Sokoto; YBS, Yobe; ZAS, Zamfara.

tient) with onset during 2005 to 2011 (2005, 4; 2006, 39; 2007, 76; 2008, 66; 2009, 156; 2010, 27; 2011, 35) include 11 from patients who were coinfected with WPV1 or WPV3. Patients with such isolates were previously excluded from our VDPV2 case counts (15) because the lower paralytic attack rates of PV2 infections than of WPV1 and WPV3 infections (45) suggested that the etiologic agents of the observed AFP cases were most likely the coinfecting WPVs. Also excluded from our analyses were cVDPV2s exported from Nigeria into Niger ($n = 6$) and Chad ($n = 1$).

Independent emergence of multiple cVDPV2 lineages. Although comparisons of VP1 region sequences (903 nt) provided a good overview of the outbreak, many of the VDPV2s were isolated soon after emergence, affording little time for divergence. Therefore, we sought to increase phylogenetic resolution among the closely related VDPV2 isolates by extending our sequence comparisons to the complete P1/capsid regions (2,637 nt) of all 2005-2011 Nigerian VDPV2 isolates (Fig. 3; see also Fig. S1 to S4 in the supplemental material). However, the relationships among time-ordered P1/capsid region sequences of all isolates were inconsistent with the polio molecular clock (47), as some isolates from more recent cases had far fewer nucleotide substitutions than isolates from earlier cases. When the outbreak was resolved into 23 separate emergences, numbered by year and within years, ordered by the estimated dates of the initiating OPV doses (see below), compatibility with a molecular clock was restored (Fig. 4 and Table 1).

Of the 23 emergences, 7 expanded into observed cVDPV2 lineage groups containing 2 to 361 isolates. The two VDPV2 isolates from the southern states of Anambra and Lagos with only moderate levels of divergence from Sabin 2 were unlike most cVDPVs (19, 32, 75) by having either nonrecombinant genomes (ANS07-01) or vaccine/vaccine (Sabin 2/Sabin 3) (LAS05-01) recombinant genomes (data not shown). Because the corresponding cases occurred in states with relatively high rates of routine tOPV coverage and signaled independent emergences with no known secondary spread, they were not considered to be part of the outbreak (15).

Assignment of isolates to independent VDPV2 emergences and lineage groups was based primarily on pairwise P1/capsid region sequence differences across emergences (Table 2) and within lineage groups (see Tables S2 to S8 in the supplemental material). Substitutions within the codon for $VP1_{143}$ were excluded from the pairwise comparisons because all VDPV2 isolates had a substitution within that codon. Other P1/capsid region substitutions were primarily synonymous changes, nearly randomly

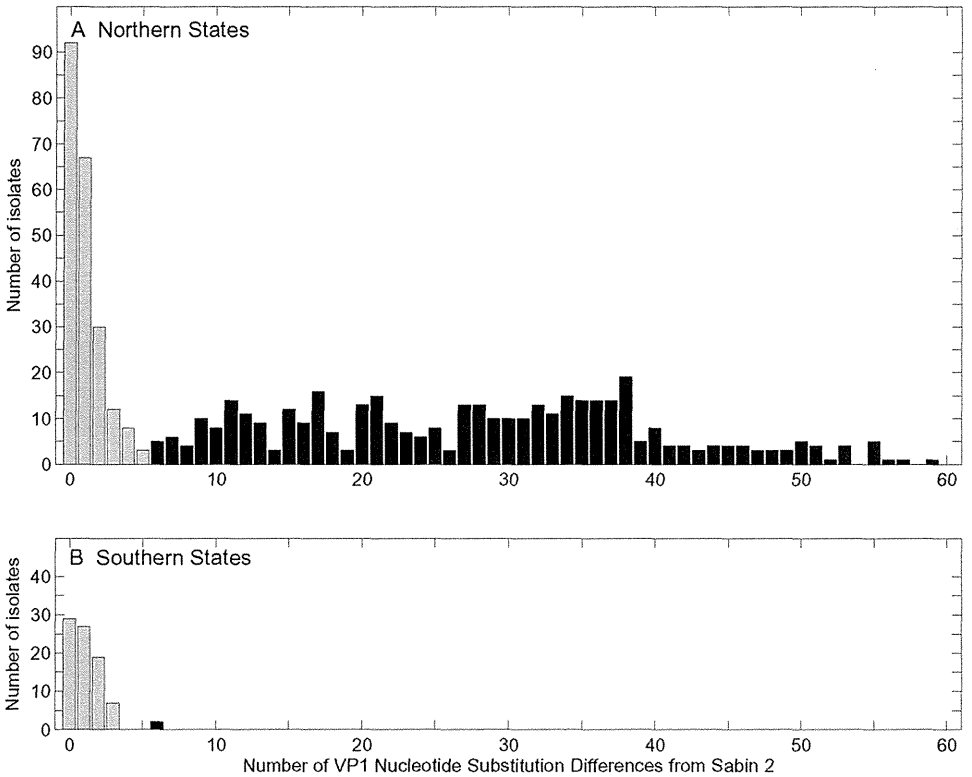

FIG 2 Distribution of nucleotide substitutions in the VP1 regions of Sabin 2-related polioviruses isolated from patients with AFP from 2005 to 2011 in the northern (n = 612) (A) and southern (n = 83) (B) states of Nigeria. Each isolate is from an individual patient. The northern and southern states are identified in Fig. 1. Type 2 vaccine-derived polioviruses (VDPV2s) (black bars) are more divergent, having ≥6 nt substitutions in the VP1 region (48).

distributed, with a different pattern of substitution for each emergence. Among the P1/capsid region nucleotide differences from Sabin 2 outside the codon for $VP1_{143}$, the proportion shared by the first isolates of each independent emergence averaged 2.4% (range, 0% to 13%), whereas the proportion shared by isolates within each lineage group averaged ~42% (range, 11% to 95%; only a subset of isolates from lineage group 2005-8 were compared) (Table 2). The common node for sequences of the two isolates of lineage group 2005-5 was so deep as to suggest that they had emerged independently. However, the two isolates shared common recombination junctions near nt 485 and 4959 and close nucleotide identities (99.2% and 98.4%) in the flanking nonvaccine sequences (see below), thus confirming their emergence from a common tOPV dose. The structure of the recombinant genomes further supported the assignment of isolates to specific emergences and lineage groups (data not shown).

When individual lineage groups were analyzed by Bayesian MCMC inference (see Fig. S1 to S4 in the supplemental material), the mean of the estimated substitution rates at all sites (K_T) for the major lineage group, 2005-8, was 1.12 (1.05 to 1.20) × 10^{-2} nt substitutions/site/year, with an average rate of 1.14 × 10^{-2} nt substitutions/site/year for the four largest lineage groups (Table 3). The values obtained for this robust data set were very close to VP1 K_T substitution rates described previously (36, 47, 57, 76, 77). Also, as previously described for WPV1 (47), synonymous transitions (A'_S) were ~10-fold more frequent than synonymous transversions (B'_S) (Table 3 and Fig. 5).

Estimated dates of VDPV2 emergences. The dates of the tOPV doses that initiated each of the 23 observed emergences were estimated from the total number of nucleotide substitutions in the P1/capsid region by assuming a constant P1/capsid K_T substitution rate of 1.1 × 10^{-2} nt substitutions/site/year throughout the period of divergence (Table 1 and Fig. 4). The estimated time interval between the initiating tOPV doses (the corresponding vaccine recipients are unknown) and the first VDPV2 isolate averaged ~9 months (range, 3 to 21 months) (Table 1 and Fig. 4), with confidence intervals (95% HPD intervals) of 7 to 15 months for the seven lineage groups. Uncertainties in the estimates were greatest for the least divergent isolates, such as BOS06-02 and ANS07-01, for which the random nature of nucleotide substitution is evident by the strong localization of substitutions to the VP1 region (Table 1), leading to nearly 3-fold-higher substitution rate estimates for the VP1 region than for the P1/capsid region. Although early selection against the Sabin 2 allele at $VP1_{143}$ (and the possible effects of any hitchhiker substitutions) may violate our assumption of a constant rate of substitution into the P1/capsid region (77, 78), the primary source of uncertainty appears to derive from the stochastic nature of the clock.

The P1/capsid region sequence tree resolving the lineage groups generally had deep nodes (Fig. 3 and Table 4; see also Fig. S1 to S4 in the supplemental material), consistent with cVDPV2 transmission soon after administration of the initiating tOPV doses. Estimates of the mean time between the initiating tOPV dose and the dates of the first divergence within each lineage group ranged between 2.0 and 6.5 months (Fig. 4 and Table 4).

The first VDPV2 isolate, BAS05-01, was isolated from a patient

COLOR

FIG 3 Maximum clade credibility subtree of P1/capsid region sequences (2,637 nt) of 62 2005-2011 isolates representing the seven well-defined cVDPV2 lineage groups (in boldface type) and 16 other isolates that signaled additional independent VDPV2 emergences (lightface type). Lineage groups and emergences are numbered by year and ordered within years by the estimated dates of the initiating OPV doses. *, VDPV2/WPV1 coinfections. Color-coding of isolate identifiers corresponds to that used in Fig. 1.

whose onset of AFP was ~10 months after the estimated time (September 2004) of the initiating tOPV dose (Table 1). Independent emergences continued for nearly 4 years, into late 2008 (Fig. 1 to 4 and Table 1). Two additional VDPV2 isolates from cases in February and November 2011 signaled more recent emergences. The initiating tOPV dose for the major cVDPV2 lineage group, 2005-8, was estimated to have been given in October 2005, more than a year after the estimated date of the initiating dose for the first observed cVDPV2 lineage group, 2004-1. The last observed cVDPV2 lineage group, 2007-5, was estimated to have emerged from a tOPV dose given in late 2007. Thus, despite widespread circulation of cVDPV2, local gaps in immunity to PV2 persisted

AQ: I